NASA/TM–2018-104606 / Vol. 49

Technical Report Series on Global Modeling and Data Assimilation, Volume 49

Randal D. Koster, Editor

Preliminary evaluation of influence of aerosols on the simulation of brightness temperature in the NASA's Goddard Earth Observing System Atmospheric Data Assimilation System

Jong Kim, Santha Akella, Arlindo M. da Silva, Ricardo Todling, and William McCarty

National Aeronautics and
Space Administration

Goddard Space Flight Center
Greenbelt, Maryland 20771

March 2018

NASA STI Program ... in Profile

Since its founding, NASA has been dedicated to the advancement of aeronautics and space science. The NASA scientific and technical information (STI) program plays a key part in helping NASA maintain this important role.

The NASA STI program operates under the auspices of the Agency Chief Information Officer. It collects, organizes, provides for archiving, and disseminates NASA's STI. The NASA STI program provides access to the NASA Aeronautics and Space Database and its public interface, the NASA Technical Report Server, thus providing one of the largest collections of aeronautical and space science STI in the world. Results are published in both non-NASA channels and by NASA in the NASA STI Report Series, which includes the following report types:

- TECHNICAL PUBLICATION. Reports of completed research or a major significant phase of research that present the results of NASA Programs and include extensive data or theoretical analysis. Includes compilations of significant scientific and technical data and information deemed to be of continuing reference value. NASA counterpart of peer-reviewed formal professional papers but has less stringent limitations on manuscript length and extent of graphic presentations.
- TECHNICAL MEMORANDUM. Scientific and technical findings that are preliminary or of specialized interest, e.g., quick release reports, working papers, and bibliographies that contain minimal annotation. Does not contain extensive analysis.
- CONTRACTOR REPORT. Scientific and technical findings by NASA-sponsored contractors and grantees.
- CONFERENCE PUBLICATION. Collected papers from scientific and technical conferences, symposia, seminars, or other meetings sponsored or co-sponsored by NASA.
- SPECIAL PUBLICATION. Scientific, technical, or historical information from NASA programs, projects, and missions, often concerned with subjects having substantial public interest.
- TECHNICAL TRANSLATION. English-language translations of foreign scientific and technical material pertinent to NASA's mission.

Specialized services also include organizing and publishing research results, distributing specialized research announcements and feeds, providing help desk and personal search support, and enabling data exchange services. For more information about the NASA STI program, see the following:

- Access the NASA STI program home page at http://www.sti.nasa.gov
- E-mail your question via the Internet to help@sti.nasa.gov
- Phone the NASA STI Information Desk at 757-864-9658
- Write to:
  NASA STI Information Desk
  Mail Stop 148
  NASA's Langley Research Center
  Hampton, VA 23681-2199

NASA/TM–2018-104606 / Vol. 49

Technical Report Series on Global Modeling and Data Assimilation, Volume 49

Randal D. Koster, Editor

Preliminary evaluation of influence of aerosols on the simulation of brightness temperature in the NASA's Goddard Earth Observing System Atmospheric Data Assimilation System

Jong Kim
Science Systems and Applications, Inc., Lanham, MD
Santha Akella
Science Systems and Applications, Inc., Lanham, MD
Arlindo M. da Silva
NASA's Goddard Space Flight Center, Greenbelt, MD
Ricardo Todling
NASA's Goddard Space Flight Center, Greenbelt, MD
William McCarty
NASA's Goddard Space Flight Center, Greenbelt, MD

National Aeronautics and
Space Administration

Goddard Space Flight Center
Greenbelt, Maryland 20771

March 2018

Level of Review: This material has been technically reviewed by technical management.

Available from

NASA STI Program
Mail Stop 148
NASA's Langley Research Center
Hampton, VA 23681-2199

National Technical Information Service
5285 Port Royal Road
Springfield, VA 22161
703-605-6000

Abstract

This document reports on preliminary results obtained when studying the impact of aerosols on the calculation of brightness temperature (BT) for satellite infrared (IR) instruments that are currently assimilated in a 3DVAR configuration of Goddard Earth Observing System (GEOS)-atmospheric data assimilation system (ADAS). A set of fifteen aerosol species simulated by the Goddard Chemistry Aerosol Radiation and Transport (GOCART) model is used to evaluate the influence of the aerosol fields on the Community Radiative Transfer Model (CRTM) calculations taking place in the observation operators of the Gridpoint Statistical Interpolation (GSI) analysis system of GEOS-ADAS. Results indicate that taking aerosols into account in the BT calculation improves the fit to observations over regions with significant amounts of dust. The cooling effect obtained with the aerosol-affected BT leads to a slight warming of the analyzed surface temperature (by about $0.5^{\circ}K$) in the tropical Atlantic ocean (off northwest Africa), whereas the effect on the air temperature aloft is negligible. In addition, this study identifies a few technical issues to be addressed in future work if aerosol-affected BT are to be implemented in reanalysis and operational settings. The computational cost of applying CRTM aerosol absorption and scattering options is too high to justify their use, given the size of the benefits obtained. Furthermore, the differentiation between clouds and aerosols in GSI cloud detection procedures needs satisfactory revision.

Contents

List of Figures

1 Introduction

Aerosols can affect climate and weather patterns by altering the atmospheric radiation balance and by affecting cloud and atmospheric optical properties (Boucher et al., 2013). In this report, we present preliminary results of a study that uses the Goddard Earth Observing System (GEOS)-atmospheric data assimilation system (ADAS) to evaluate the impact of aerosols on atmospheric data assimilation and radiative transfer.

At least two operational centers, namely the Naval Research Laboratory (NRL) and the European Center for Medium-Range Weather Forecasts (ECMWF), assimilate retrievals of Aerosol Optical Depth (AOD) from the MODerate Resolution Imaging Spectroradiometer (MODIS) on the AQUA and TERRA satellites (see Morcrette et al. 2009 and Lynch et al. 2016). In GEOS-ADAS, the GEOS-atmospheric general circulation model (AGCM) is coupled to the Goddard Chemistry Aerosol Radiation and Transport (GOCART) component, which allows the aerosols followed in the latter to interact with the AGCM's radiation and clouds (Colarco et al., 2010). Assimilation of aerosols follows Randles et al. (2016) and is based on the Local Displacement Ensemble (LDE) strategy combined with AOD analyses produced by Goddard Aerosol Analysis System (GAAS). In its current configuration, the meteorological analysis of GEOS-ADAS does not make use of the background aerosol fields in the atmospheric data assimilation process. Hence the Gridpoint Statistical Interpolation (GSI) atmospheric analysis is made *blind* to the presence of aerosols, even though the underlying meteorology feels their effect. The present study enables GSI to account for the influence of aerosols in its radiance observation operator when simulating brightness temperature (BT) with CRTM. In addition to providing an assessment of the impact of aerosols on BT, we present a few technical issues that need to be addressed in the future for the viable use of the aerosol absorption and scattering calculations of the CRTM in reanalysis and operational applications.

Past studies have shown that aerosols significantly impact the simulation of BT in the infrared (IR). Weaver et al. (2003) studied the impact of mineral dust on the BT calculation for the High resolution Infrared Radiation Sounder (HIRS). They found that the HIRS channels that are sensitive to surface temperature, lower tropospheric temperature, and moisture were subject to a $0.5^{\circ}K$ or more reduction in BT during heavy dust loading conditions. They also reported that accounting for dust absorption in the TIROS Operational Vertical Sounder (TOVS) retrieval system resulted in a warming effect on the surface temperatures ($0.4^{\circ}K$) and warming of lower tropospheric temperatures in the *moderate* dust loading regions over the tropical Atlantic. Pierangelo et al. (2004) and Peyridieu et al. (2009) found that the dust signature may reach $3^{\circ}K$ in tropical atmospheric conditions and that its impact increases with AOD and altitude of dust. In addition, they showed that shortwave channels ($3 \sim 5\ \mu m$) are sensitive to total AOD and that long-wave channels ($8 \sim 12\ \mu m$) are more sensitive to dust altitude. For sea surface temperature (SST) retrievals, these IR channels have been used to detect and isolate the effect of dust. Merchant et al. (2006) showed that dust-sensitive IR channels can be used to develop an empirical correction scheme for SST retrievals affected by Saharan dust.

Here, we extend previous studies of aerosol impacts on BT simulation to include the following IR satellite instruments that are currently assimilated in the GEOS-ADAS: Advanced Infrared Sounder (AIRS) on AQUA, Infrared Atmospheric Sounding Interferometer (IASI) on METOP-A and METOP-B, Cross-track Infrared Sounder (CrIS) on S-NPP, HIRS on METOP-A, METOP-B, NOAA-18, and NOAA-19, Advanced Very High Resolution Radiometer (AVHRR) on NOAA-18, METOP-A and Spinning Enhanced Visible and Infrared Imager (SEVIRI) on M10. In the BT

simulation in which we account for aerosols, all GOCART-based aerosol species[1], including dust, sulfate, black carbon (BC), organic carbon (OC), and sea-salt aerosols, are utilized, and the impact of each individual aerosol species on BT is evaluated. Following a brief system description in section 2, we introduce the experimental setup in section 3. Discussion of the experimental results and conclusions follow in sections 4 and 5, respectively.

2 Brief Recap of GEOS-ADAS and its Aerosol Component

The version of GEOS-ADAS used in this work is configured as a 3D-Var system using an Incremental Analysis Update (IAU; Bloom et al. 1996) approach to initialize the model background and forecast integrations. The two main components of this system are the NASA GEOS-AGCM and the multi-partner-developed Grid-point Statistical Interpolation (GSI; Kleist et al. 2009). To a large extent, the meteorological analysis, the model hydrodynamics, and the physical parameterizations of the system used in the present work are similar to those in MERRA-2 (Gelaro and coauthors 2017), with the difference that experiments here are done at higher resolution - consistent with the GMAO near-real-time system implemented in our Forward Processing (FP) system in mid 2015. Of specific relevance to the present work is the inclusion of radiatively active GOCART aerosol coupling (also present in MERRA-2; Randles et al. 2016, Buchard et al. 2015). The GAAS component uses the Physical-space Statistical Analysis System (PSAS) for updating AOD. De-biased observations from several ground- and satellite-based sensors including the AVHRR over ocean, MODIS on both TERRA and AQUA satellites, MISR over bright surfaces, and the Aerosol Robotic Network (AERONET) over both land and ocean are used to analyze the 550 μm AOD. The AOD analysis is produced on a three-hourly basis, and the fifteen aerosol species of GOCART are updated with the LDE approach combined with an averaging-kernel methodology to allow for a three-hourly intermittent update of the full three-dimensional GOCART aerosol fields. This update takes place during the corrector phase of IAU, when the six-hourly analysis tendency is used to initialize the model with the 3D-Var solution of GSI.

The aerosol species included in this work are similar to those in Buchard et al. 2015 and include hydrophobic- and hydrophilic-black and -organic carbon, dust, sea salt, and sulfates with five bins of different particle sizes for dust and sea-salt, and four bins for sulfates. In its 3D-Var version, GSI employs a First-Guess at the Appropriate Time (FGAT) strategy (Massart et al. 2010), which amounts to requiring three-hourly backgrounds of typical meteorological fields (i.e., temperature, winds, pressure, etc). For consistency with FGAT, three-hourly aerosol background fields are made available to GSI so that it can accurately perform its aerosol-influenced BT calculations in the experiments described below in section 3. Specifically, given an atmospheric profile of temperature, variable gas and aerosol concentrations, and cloud and surface properties, CRTM is called within the GSI to calculate brightness temperatures. As a fast radiative transfer model, CRTM provides accurate simulations for many satellite instruments from IR sounders to MW imagers. Aerosol scattering and absorption options are available from CRTM version 2.2 onwards (Liu et al., 2007); here, we used version 2.2.1. The present work focuses on IR instruments only, largely because MW measurements are unaffected by aerosols; evaluation of changes in the Jacobians of BT with respect to the atmospheric fields will be addressed in future work.

[1] At the time of this writing, three nitrate varieties have been added to GOCART; these, however, are not part of the present work.

3 Experimental Setup and Aerosol Fields

The experiments reported in this work have been produced with version 5.13.2 of GEOS-ADAS. This is the last release of a non-hybrid version of the GMAO FP system. Relative to standard FP simulations, our experiment uses coarser resolution model and analysis runs: the GEOS-AGCM runs at C360 (cubed-grid, roughly 25 km; e.g., Putman and Lin 2007); the GSI analysis runs on a regular latitude-longitude grid of roughly 50 km, the PSAS-based AOD analysis runs on a regular grid of resolution comparable to the model's 25 km resolution; the LDE update of the aerosol species is done on the model's full resolution (C360, cubed-grid). Experiments cover the month of August 2016, when considerable aerosol activity is observed, particularly off the West Coast of Africa.

The control experiment (CTL) runs the default GSI configuration, for which GSI is aerosol-blind. This fully cycled experiment is used as a baseline for comparison as well as for storage of meteorology and aerosol background fields that are used in an offline set of GSI analysis experiments. In these offline experiments, referred to as AER, GOCART aerosols are made available to the observation operator and are used in the calculation of BTs through CRTM. In this framework, where the AER offline analyses do not feed back to the cycling ADAS, it can be safely assumed that differences between the AER analyses and the CTL analyses are solely due to the CRTM aerosol-related calculations.

The AER experiments are performed only for the 12:00 UTC analysis times. The FGAT nature of GSI requires the availability of background fields at 09:00 UTC, 12:00 UTC and 15:00 UTC. In AER, the application of CRTM aerosol absorption and scattering is restricted to IR instruments handled by GSI, namely, AIRS, AVHRR, CrIS, HIRS, IASI, and SEVIRI. All fifteen GOCART aerosols are passed along to CRTM. The GSI-FGAT framework applies spatio-temporal interpolation to derive aerosol background information at the location and time of each satellite observation. A default CRTM reference lookup-table (Liu et al., 2007) is used for pre-calculated aerosol optical property parameters such as dry mass extinction, single scattering albedo, and asymmetry factor.

Figure 1 shows the global monthly-mean aerosol column mass (cMass) distribution during August 2016. Strong dust plumes are seen over northern Africa and over the tropical Atlantic Ocean. Sulfate and carbonaceous aerosol species mainly appear in areas with extensive fuel combustion and biomass burning. Wind-driven sea salt spreads over tropical and southern hemisphere ocean. Figure 2 shows the vertical monthly mean aerosol areal mass density distribution in four representative aerosol active regions. During the experimental time period, high aerosol activity is seen in the dust active region. The aerosol cMass values in the tropical area of the Atlantic ocean off of northwestern Africa are about 10 times or more higher than those of other aerosol active areas. Note that organic carbon (OC) and black carbon (BC) areal mass densities are combined here into a single carbonaceous aerosol areal mass density. In dust and carbonaceous dominant regions, the aerosols are lifted up to about 600 hPa and are transported over the Atlantic ocean. In the active sulfate and sea salt areas examined, the aerosol mass density values at high altitude are not as high as those indicated for dust and carbonaceous aerosols.

In a dust altitude and infrared optical depth retrieval study, Pierangelo et al. (2004) demonstrated that dust layer altitudes, surface emissivities, and size distributions are the key parameters in an AIRS BT calculation. In particular, they showed that the BT calculation for AIRS channels 9 to 14 μm wavelength is strongly affected by dust elevation. In our system, although GAAS does not infer the vertical distribution of each of the aerosol species in the CTL experiment, Buchard et al. (2015, 2016) have shown that the LDE update of the species in our system produces rather reliable three-dimensional aerosol features. Specifically, these authors have shown that the vertical structure of GEOS-ADAS aerosols compares favorably with independent products from the Cloud Aerosol Lidar with Orthogonal Polarization (CALIOP) instrument aboard the NASA A-Train CALIPSO

satellite.

In the presentation that follows, we concentrate on the overall statistical impact of using aerosols in the GSI analysis. A detailed sensitivity study to investigate the aerosol-affected GSI analysis in the cycling ADAS runs is left to a future study.

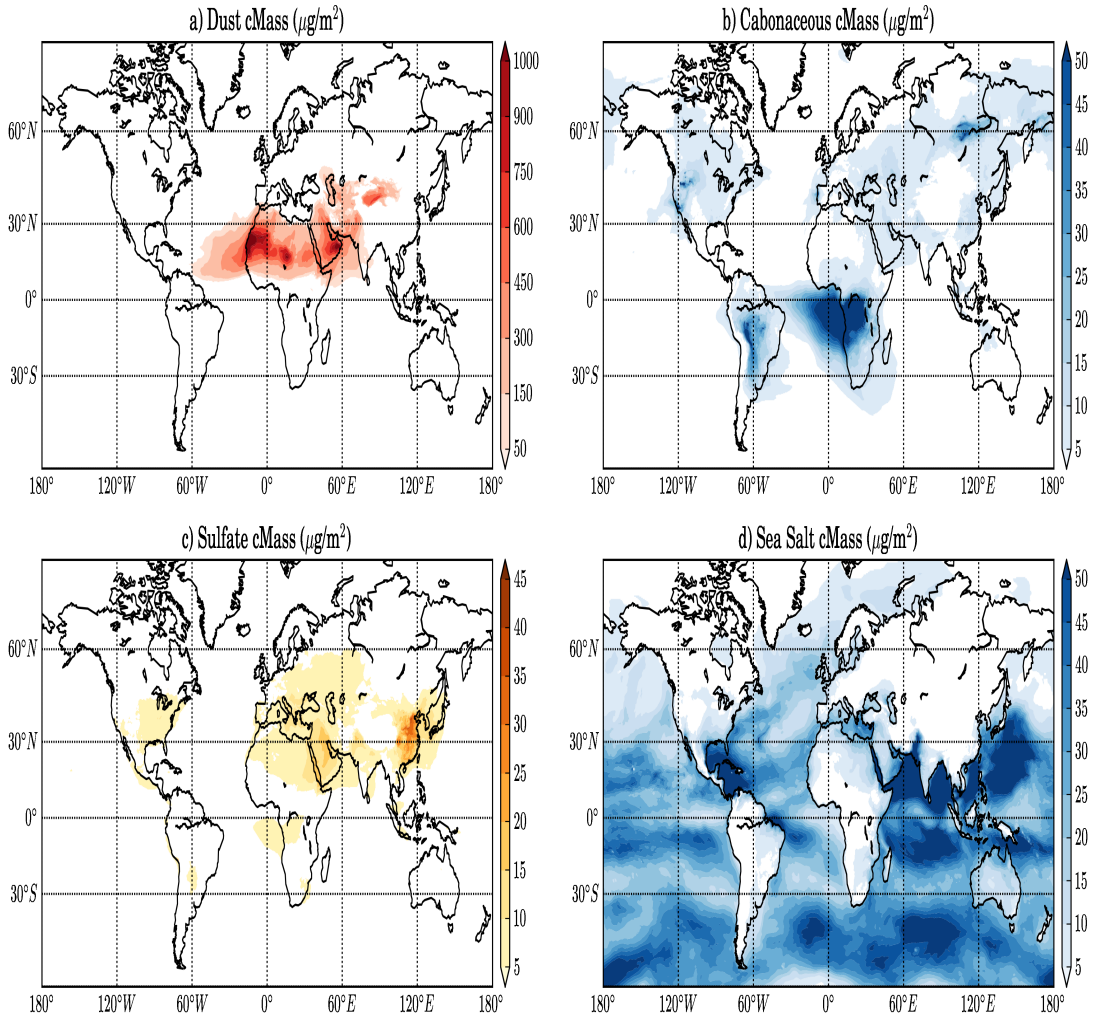

Figure 1: Global distribution of aerosol column mass (cMass in $\mu g/m^2$) during August, 2016. Panels a) ~ d) depict dust, carbonaceous, sulfate and sea salt respectively. Note the difference in scales.

4 Results

In this section, we compare the results of the AER experiments with those of the CTL analyses. We remind the reader that differences are only examined for the 12:00 UTC analyses. We start by presenting the differences found in BT. We then describe the corresponding differences in the ob-

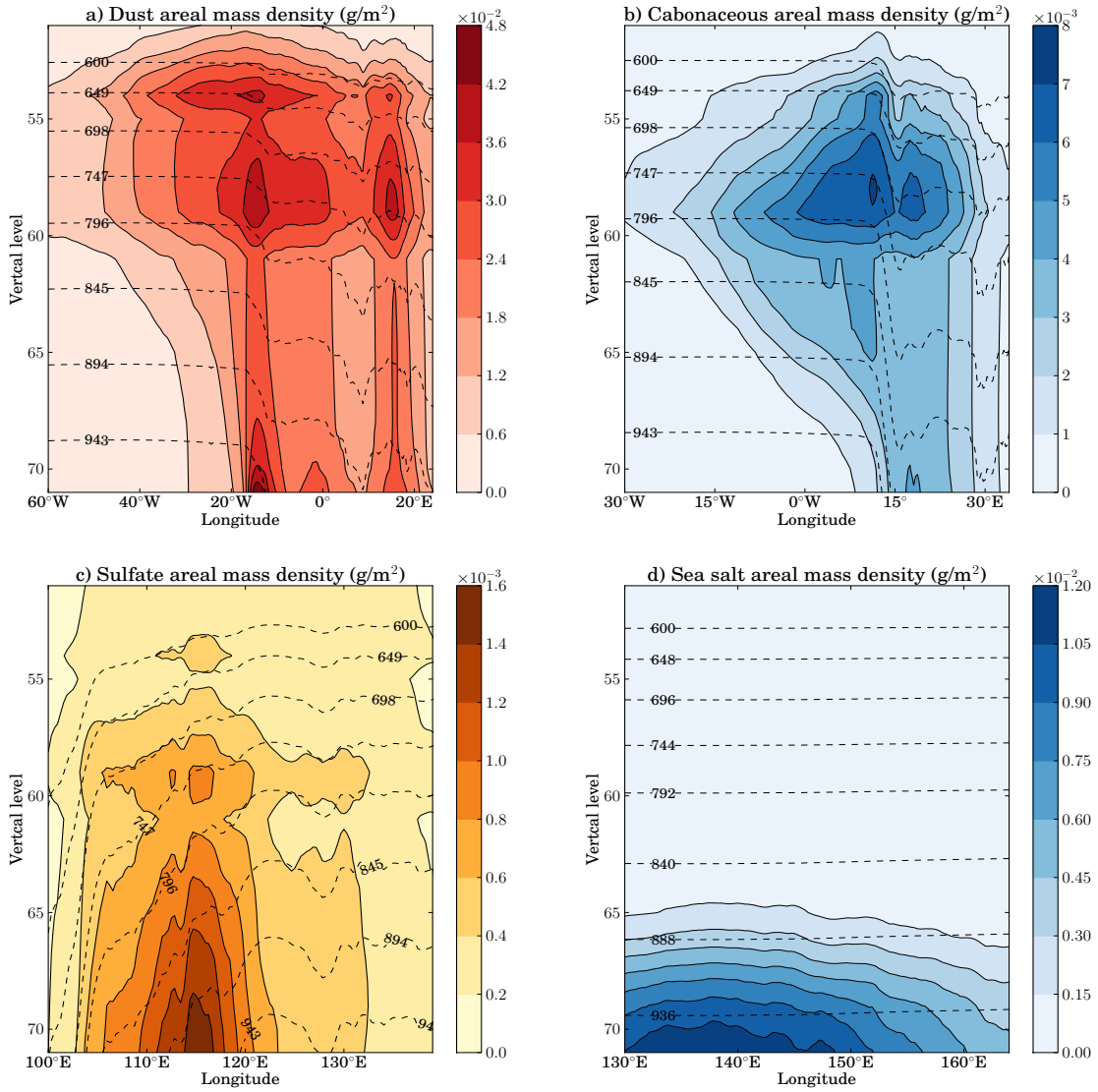

Figure 2: Vertical distribution of aerosol areal mass density (g/m^2) in selected regions of interest during August 2016: a) dust b) carbonaceous c) sulfate, and d) sea salt. Densities are shown as a function of longitude and height; the latitudes over which they are averaged are 10^oN to 25^oN for dust, 20^oS to 0^oN for carbonaceous, 25^oN to 45^oN for sulfate, and 10^oN to 20^oN for sea salt. Note the difference in color scales. Contours show pressure levels. See text for details.

servational residual statistics - i.e., observation-minus-background (OMB) and observation-minus-analysis (OMA). We next discuss the differences found in the analyzed fields themselves and finally offer some brief comments on computational cost as related to CRTM's aerosol absorption and scattering calculations.

4.1 Change in brightness temperatures

We determine the difference in the brightness temperatures between CTL and AER, $\mathrm{BT}_{CTL} - \mathrm{BT}_{AER}$, for each channel of the IR instruments. Positive values indicate that a cooling effect is

introduced in the AER experiment. Due to the uncertainties in the CRTM land surface emissivity, we focus here only on ocean data points. The global monthly-mean BT differences between the CTL and AER experiments are shown in Figure 3. While all of the IR instruments show a cooling effect, the cooling varies slightly based on orbital characteristics and instrument (channel) specifications. The maximum cooling is about $0.15^{\circ}K$ around the $10\mu m$ channels for IASI and SEVIRI. For other instruments, maximum values are about $0.1^{\circ}K$. Although some shortwave (near $4\mu m$) channels show a considerable cooling effect as well, we consistently observe that the 8 to $12\mu m$ wavelength channels show the most sensitive response to the aerosol fields used in AER experiment. Pierangelo et al. (2004) and Peyridieu et al. (2009) reported a similar cooling effect for the AIRS instrument, though they tested only dust cases and used a different radiative transfer model.

In an attempt to relate the above differences in brightness temperatures to aerosol type and amount, we *stratify* the BT differences between the CTL and AER experiments by introducing a fractional mass, cMass, of each aerosol species, i, as follows:

$$cMass_{frac,i} = \frac{cMass_i}{cMass_{total}}$$

Four different stratifications are made here, one for each aerosol type: dust, carbonaceous, sulfate, and sea salt. In each stratification, only those data points that meet the background aerosol stratification condition of $cMass_{frac,i} > 0.65$ for that type over the ocean are counted. (In general, the conclusions from these evaluations were not very sensitive to the 0.65 threshold; naturally, decreasing it increased the averaging area, whereas increasing it decreased the averaging area.) The stratification approach allows us to compare the contributions of the different aerosol species to the BT cooling effect obtained in the AER experiment. Figures 4 ~ 7 show, respectively, the stratification with respect to dust, carbonaceous, sulfates and sea salt. The right column of each figure shows the monthly mean absorptive and total AOD computed for the stratified data points of the IASI and

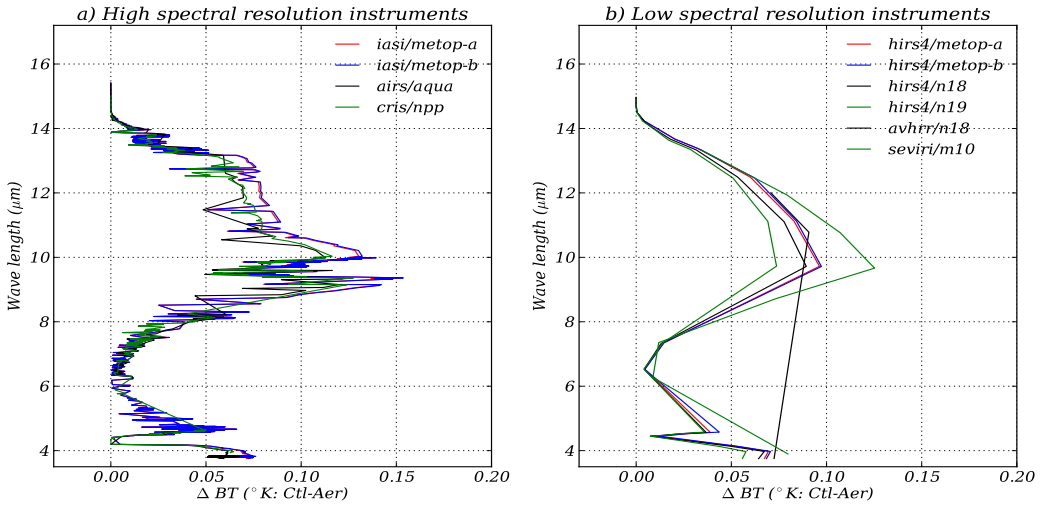

Figure 3: Monthly mean BT ($^{\circ}K$) difference between CTL and AER experiments during August, 2016, globally averaged over all data points over ocean. Left panel shows the differences for high spectral resolution instruments, and right panel shows the differences for lower resolution instruments.

HIRS channels. The overall BT cooling effect observed in Figure 3 is similarly reflected in the results of each stratification.

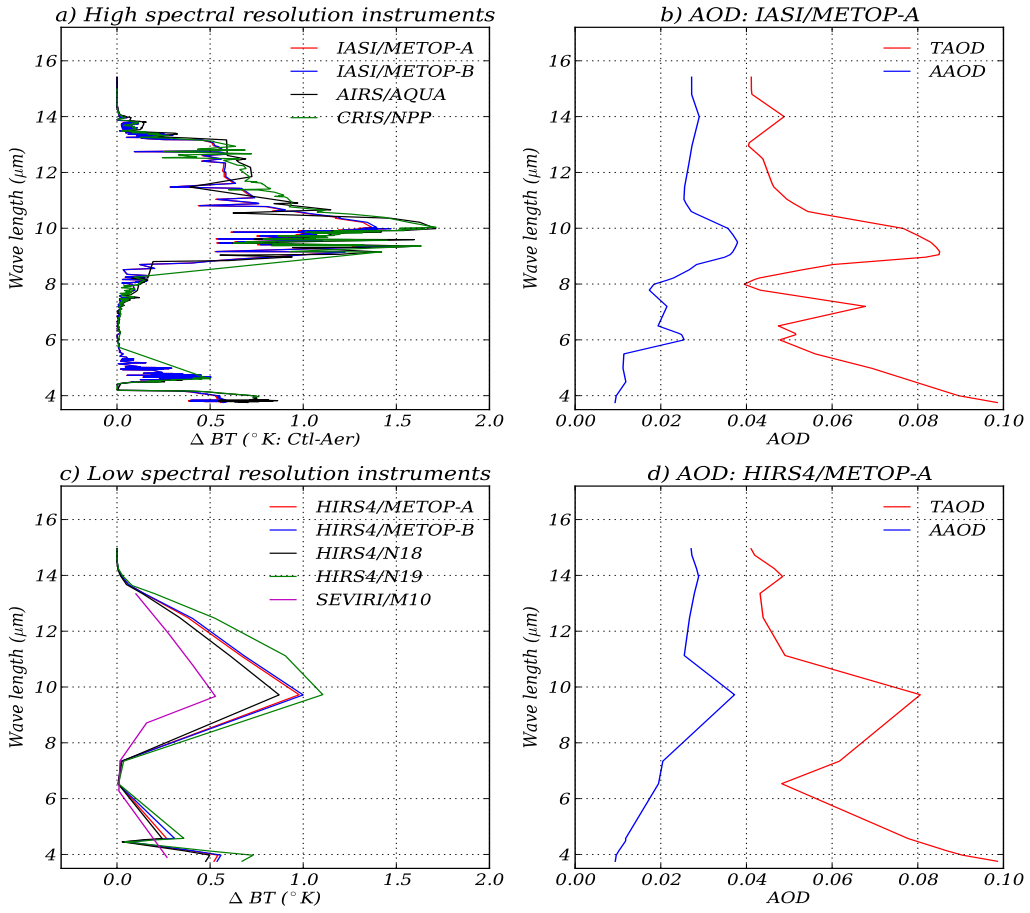

Figure 4: (left panels) Monthly mean BT ($^{\circ}K$) difference between CTL and AER experiments and computed AOD during August, 2016, as computed over ocean points for which dust cMass$_{frac} >$ 0.65) (see Figure 1). (right panels) Corresponding monthly mean Absorptive AOD (AAOD) and Total AOD (TAOD).

Figure 4 shows that most of the BT cooling effect in the AER experiment is generated from dust regions. The cooling effect of the dust dominant region reaches about $1.5^{\circ}K$ for (roughly) the 8 to 12μm wavelength channels. In addition, we observe a positive correlation between the BT cooling effect and the total AOD values in Figure 4. Panels 4b and 4d show a sharp increase of both absorptive and total AODs in the dust sensitive channels. A relatively smaller cooling effect of about $0.7^{\circ}K$ is observed in shortwave channels in which absorptive AODs make up a smaller fraction of total AODs. Pierangelo et al. (2004) and Peyridieu et al. (2009) reported that dust elevation is strongly related to the magnitude of the BT cooling effect in the 8 to 12μm channels. Similarly, Figures 2 and 4 show that the high altitude dust over the tropical Atlantic ocean contributes considerably to the strong cooling effect in those channels.

In our experimental time period, the next most dominant aerosol species are carbonaceous and

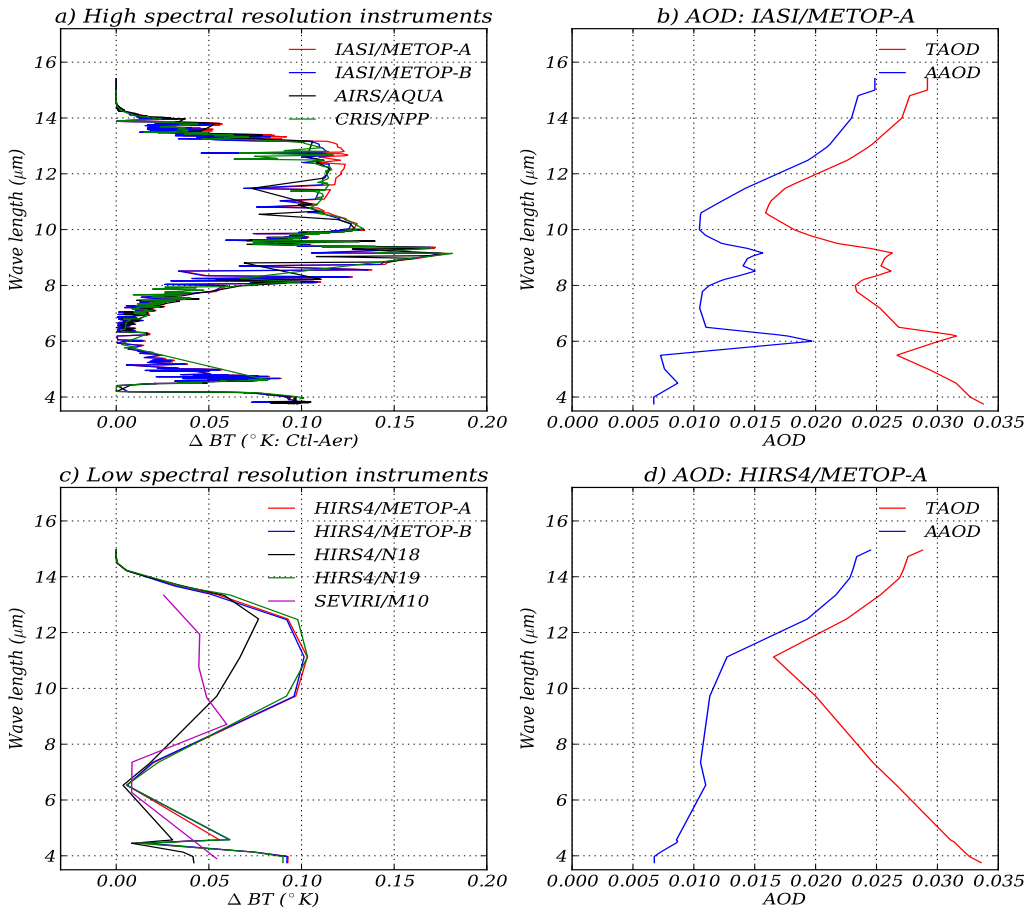

Figure 5: Same as Figure 4, but over ocean points for which carbonaceous aerosols dominate (BC+OC cMass$_{frac} > 0.65$).

sulfate aerosols, which result from active biomass burning in central Africa. Relatively high sulfate concentrations can also be seen in East Asia (see Figures 1 and 2). Figure 5 shows that the cooling effect of the AER experiment in the regions dominated by carbonaceous aerosol is about $0.15°K$ for the 8 to $12\mu m$ wavelength channels. On a somewhat smaller scale, a similar cooling behavior is shown in Figure 6 for the sulfate stratification. Compared to the dust stratification case, the long-wave channels of about 12 to $14\mu m$ wavelength are slightly more sensitive to the carbonaceous and sulfate aerosol species. With regard to the correlation between the BT cooling effect and the AODs, a relatively weak correlation is captured near the channels around 8 to $12\mu m$ wavelength. Finally, Figure 7 shows that sea salt aerosol has the smallest impact on the BT calculation, with a very weak correlation between the BT cooling effect and the computed AODs.

4.1.1 Impact of dust

As shown above, dust species cause the largest differences in BT between the CTL and AER experiments. Intensive dust activity over ocean grid points provides a good opportunity to compare

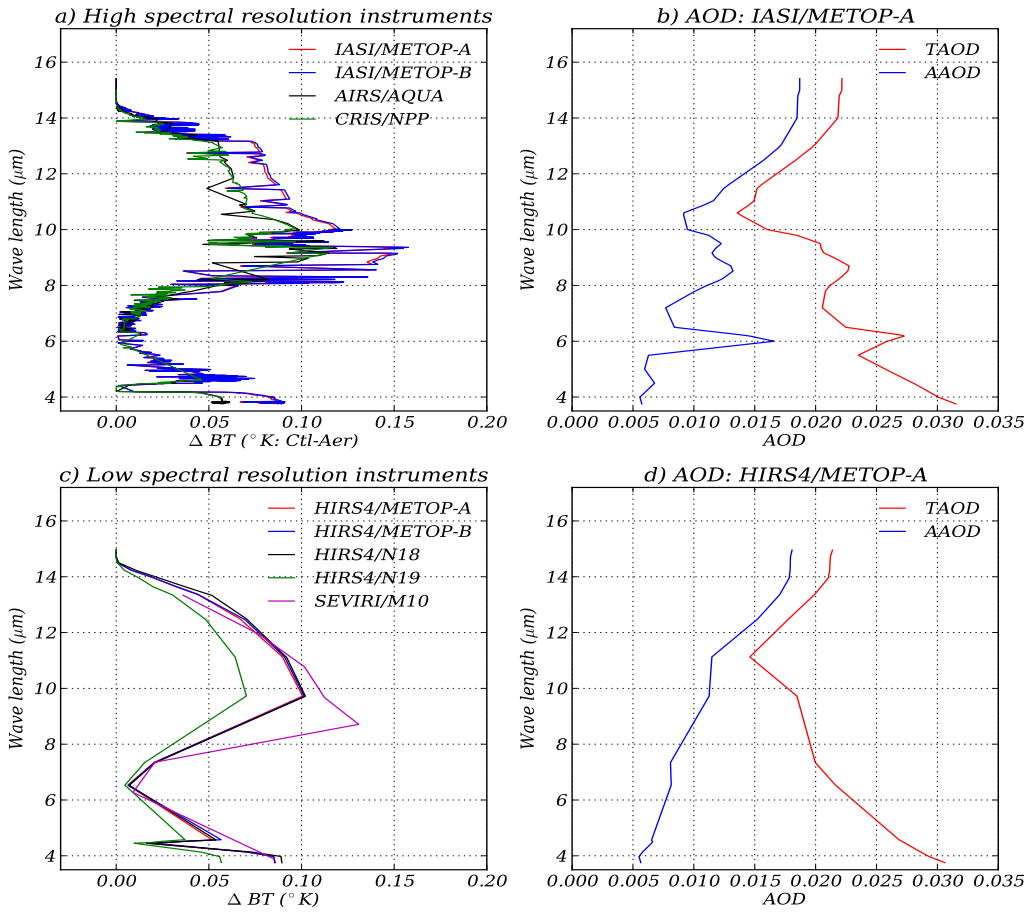

Figure 6: Same as Figure 4, but over ocean points for which sulfate aerosol dominates (SO_4 $\text{cMass}_{frac} > 0.65$).

our BT computational results with observed data. Here we focus on a dust active region to make a direct comparison of our calculated BTs with observational data from a high spectral resolution instrument. Observed and calculated BTs for the $10.38\mu m$ wavelength channel of IASI are shown in Figure 8.

The maps of computed BTs in Figure 8 clearly show that the AER experiment represents well the dust-affected BT observational data shown in Figure 8b, especially over the Atlantic ocean (e.g., around the area of 40N). Since dust does not impact the BT calculation in the CTL experiment, the BT calculation for CTL produces overestimated values in dust active regions. While the calculated BTs in the AER experiment shown in Figure 8d range from $292°K$ to $294°K$ in the dust active area, the CTL experiment's TBs constantly remain over $295°K$. Panels 8c and 8d include all data points before the quality control (QC) and bias correction processes of the GEOS-ADAS. In the QC process, a clear-sky criteria is applied to remove the cloud-contaminated satellite radiance data. It turns out that a significant portion of IR observation data are cleared during the QC and bias correction processes in both experiments. Figures 8e and 8f show the calculated BT results after QC and bias correction. Figures 8g and 8h show the BT data points rejected due to cloud contamination;

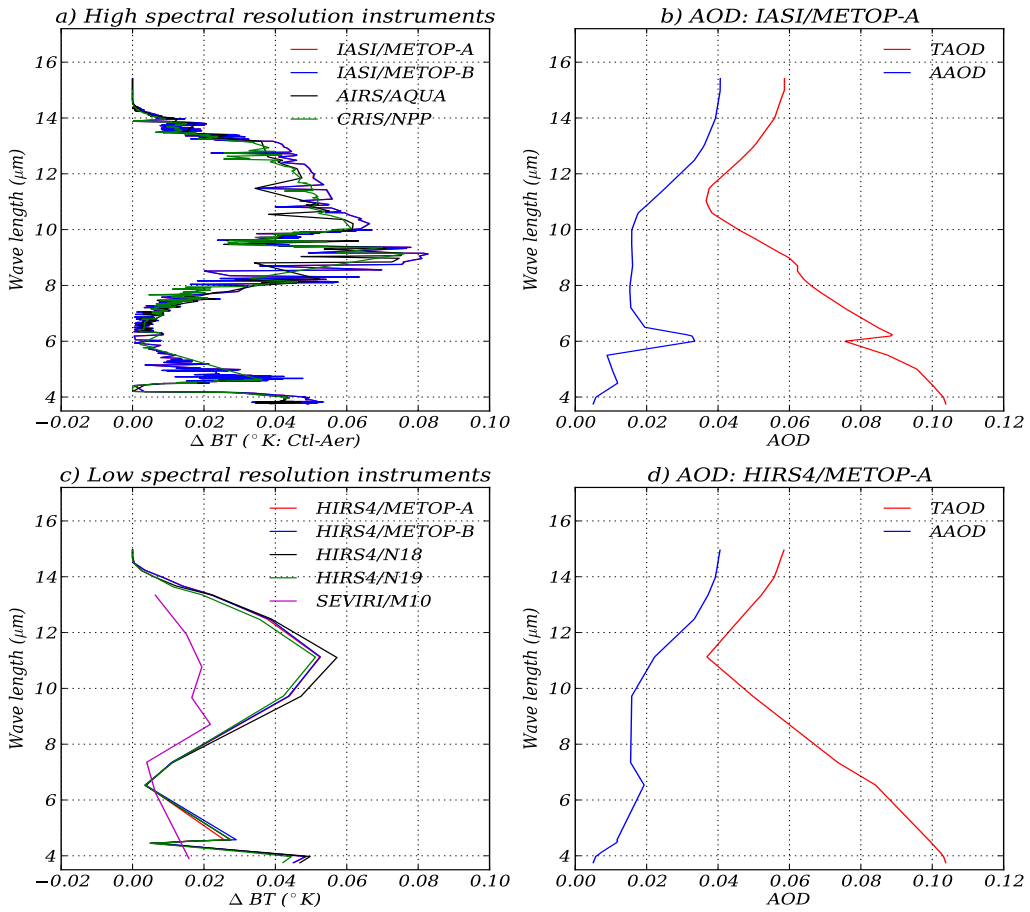

Figure 7: Same as Figure 4, but over ocean points for which sea salt dominates (sea salt cMass$_{frac} >$ 0.65).

as expected, a considerable number of data points were rejected, especially in the dust active region. In this sense, an improved QC approach that distinguishes between cloud and aerosol signals may allow aerosol impacts on the BT calculation to be investigated with more data points; however, development of such an improved QC approach is beyond the scope of this study. Even given the technical issue of cloud contamination, Figs.8e and 8f show that the AER experiment accepts a few more data points than CTL in the dust-affected region.

4.2 Change in observational residuals

Since dust has the largest impact on the BT computation, we now compare the observation-minus-background (OMB) statistics of the CTL and AER experiments in areas dominated by dust (dust cMass$_{frac} > 0.65$). Figure 9 shows the monthly mean OMBs of the CTL and AER experiments before QC and bias correction for high spectral resolution IR instruments. Over a broad range of wavelengths, the dust cooling effect on the BT calculation consistently improves the monthly mean OMB for all instruments.

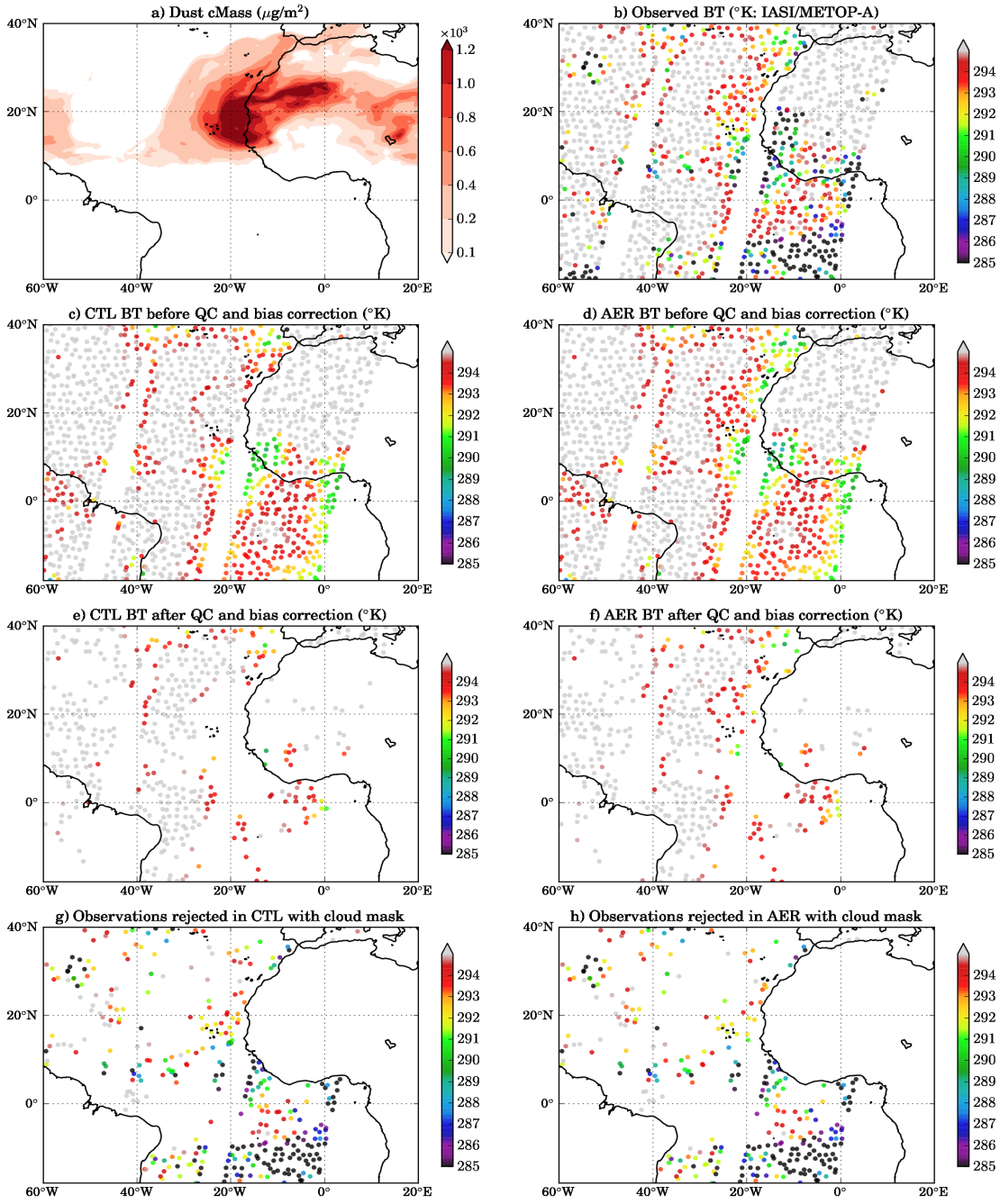

Figure 8: Comparison of the computed BTs with observation data from the 10.38μm wavelength channel of IASI/METOP-A during August 29 (12:00 UTC), 2016: a) horizontal distribution of dust cMass, b) observed BT, c) computed BT from the CTL experiment, d) computed BT from the AER experiment before QC and bias correction, e) computed BT from the CTL experiment after QC and bias correction, f) computed BT from the AER experiment after QC and bias correction, g) BT data points rejected due to cloud contamination criteria in the CTL experiment, and h) BT data points rejected due to cloud contamination criteria in the AER experiment.

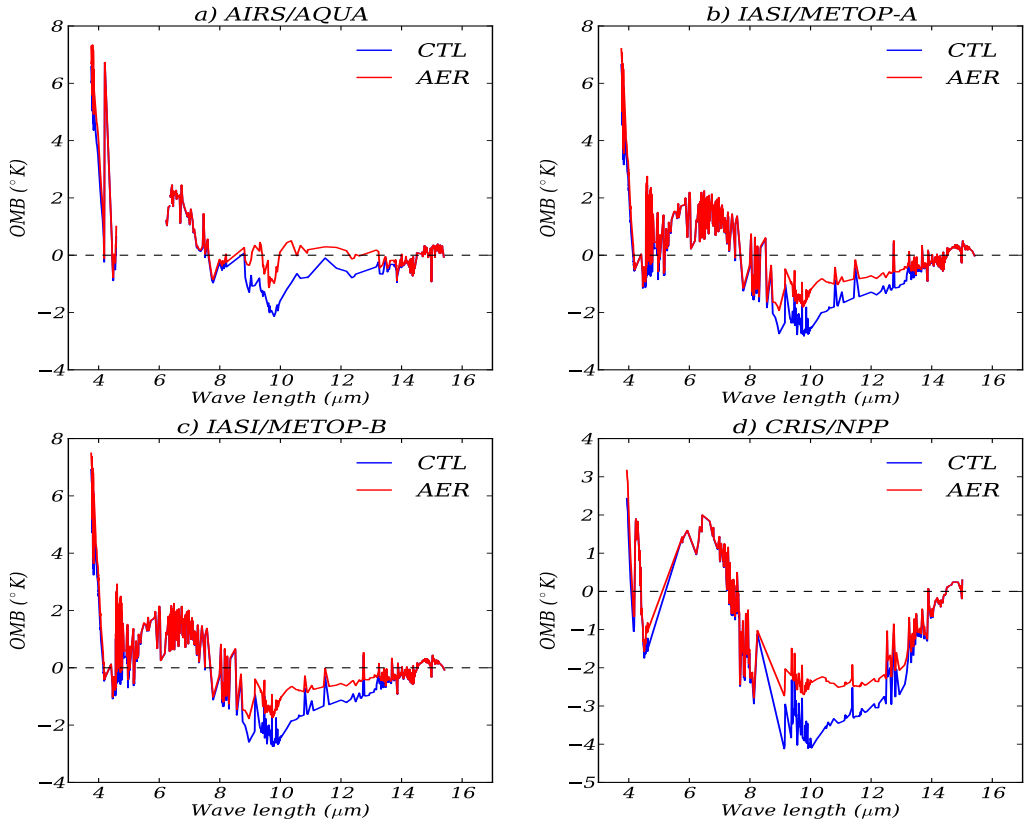

Figure 9: Monthly mean OMB before QC and bias correction for the data points dominated by dust (dust cMass$_{frac} > 0.65$) during August (12:00UTC), 2016: a) AIRS/AQUA, b)IASI/METOP-A, c) IASI/METOP-B, and d) CrIS/NPP

For the channels of CrIS having negative OMB bias, the calculated BTs of the AER experiment get closer to observational data by up to $2°K$. In the range of 8 to $14\mu m$ wavelength, the negative OMB bias is considerably mitigated for most instruments. The improvement is especially pronounced near the $10\mu m$ wavelength. Compared to the other instruments, CrIS benefits the most from the AER experiment before QC and bias correction processes.

Figure 10 shows the monthly mean OMB after QC and bias-correction. The dust stratification is applied in the same way as in previous figures. In a considerable portion of the negatively biased channels between 7 and 11 μm wavelengths, the mean OMB values are improved even after QC and bias correction. In particular, noticeable improvement is found near the $10\mu m$ channels of various instruments.

However, some exceptions are found; the positive impact of the aerosol-affected BT computation is not always carried into improving the mean OMBs after QC and bias correction. For some channels of AIRS and IASI instruments, the aerosol cooling effect in the AER experiment causes an increased positive OMB bias after QC and bias correction.

The standard deviations of the OMBs after QC and bias correction are shown in Figure 11. While not much difference is found between the figures for the AIRS and IASI instruments, noticeably lower OMB standard deviation values are obtained in the AER experiment for a broad range

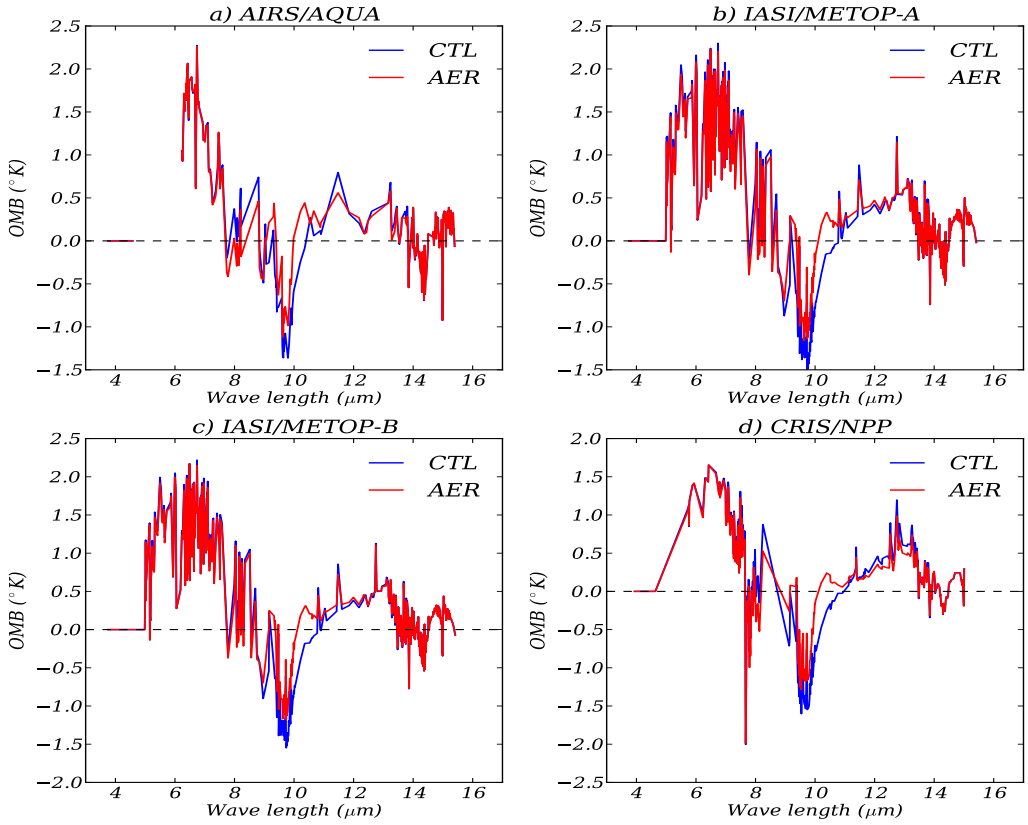

Figure 10: Same as Figure 9, but after QC and bias correction.

of the channels of CrIS. This indicates that the BT cooling effect of the AER experiment allows a narrower OMB distribution even after QC and bias correction. In Figure 12, we compare the histograms of the OMB for the AER and CTL experiments. As the most beneficial impact of the AER experiment is found for channels near $10\mu m$, we select one of these channels currently in use in GEOS-ADAS. For all high spectral resolution instruments, the negative bias of the OMB is considerably reduced in the AER experiment.

Figure 13 shows the monthly mean difference of the total number of the assimilated data counts in the CTL and AER experiments. Only channels currently assimilated in the CTL and AER experiments are included in the figure. Positive numbers mean that more observational data are assimilated in the AER experiment. While the data count difference between the two experiments is not significant, the AER experiment generally accepts slightly more data. In particular, more data is assimilated in the AER experiment for a significant portion of the aerosol-sensitive channels around the 10 to $14\mu m$ wavelength band.

4.3 Impact on analysis fields

Before we discuss the differences in analysis fields with and without the impact of aerosols, we compare the observation-minus-analysis (OMA) residuals for the CTL and AER experiments for select surface sensitive window channels of the high spectral resolution instruments (AIRS/AQUA,

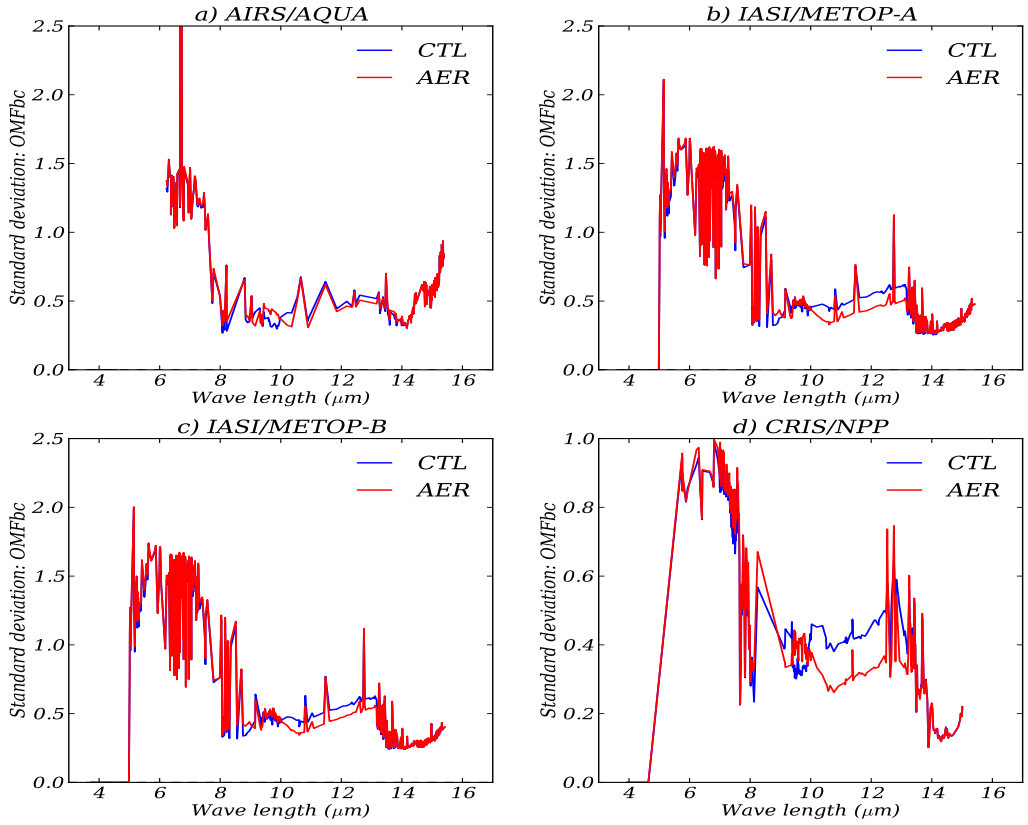

Figure 11: Monthly mean standard deviation of OMB after QC and bias correction for the data points dominated by dust (Dust cMass$_{frac} > 0.65$) during August (12:00UTC), 2016: a) AIRS/AQUA, b)IASI/METOP-A, c) IASI/METOP-B, and d) CrIS/NPP

CrIS/NPP and IASI on METOP-A and METOP-B) discussed thus far. Figure 14 shows the monthly mean OMA (obtained after QC and no bias correction) binned to regular 5^o grid resolution for the $11.9\mu m$ channel of AIRS/AQUA. Consistent with the earlier evaluations, we focus on the dust-active Atlantic region. As discussed above (Figure 13), the AER accepts a slightly larger number of observations in this region. However, there is also a slight increase, of about 0.1K to 0.2K, in mean OMA, which is consistent with the warm bias shown in Figure 10(a). Since the AER experiment is conducted offline (section 3), where bias correction does not get evolved, we do not compare bias corrected OMA residuals. A similar result is obtained for IASI/METOP-A channel $10.4\mu m$, as shown in Figure 15. For CrIS/NPP, both CTL and AER are similar to each other; see Figure 16. Consistent with previous results (Figures 3 ~ 13), the OMA residual statistic for the IASI on METOP-A is similar to that for METOP-B and is thus not shown here. Also, a similar result is obtained for all other surface sensitive IR (window) channels in the $10 \sim 12\mu m$ wavelength range.

Based on these results we speculate that the simulated BT from the analysis fields (skin and virtual temperatures, winds, moisture) for the surface sensitive channels is farther away from the observations than that from the background fields. The analyzed BT in AER is colder than that in CTL, which is analogous to results of the simulation of BTs from the background fields discussed in section 4.2. This effect is directly attributable to the aerosol influence in the BT simulations of

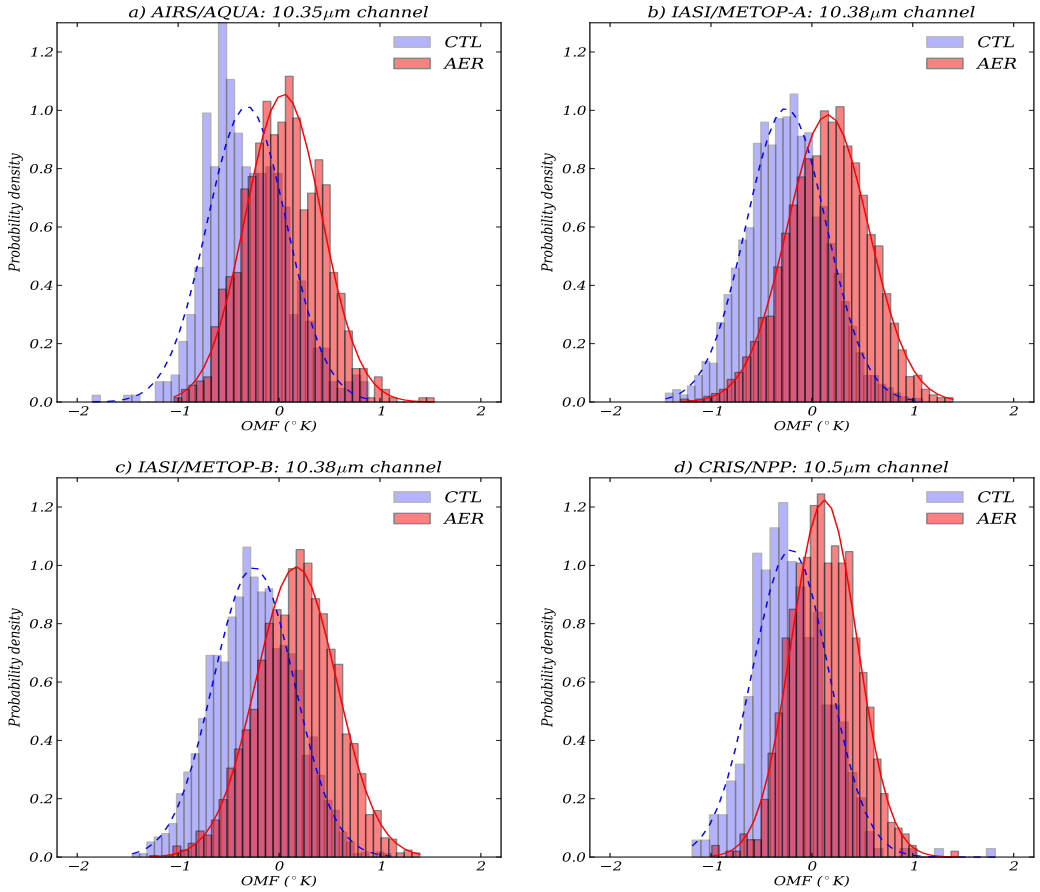

Figure 12: Histograms of OMB after QC and bias correction for the assimilated data points with dust stratification (Dust cMass$_{frac} > 0.65$) during August (12:00UTC), 2016: a) AIRS/AQUA, b)IASI/METOP-A, c) IASI/METOP-B, and d) CrIS/NPP.

the AER experiment.

Regardless of the above limitations, we now discuss the differences in the analyzed temperatures. Figure 17 shows the monthly mean analysis temperature difference between the CTL and AER experiments, calculated as $T_{AER} - T_{CTL}$. Positive values imply a warming up effect caused by the AER experiment. In the monthly mean surface temperature difference, land grid points are masked out because only the ocean skin temperature analysis option is being used in GEOS-ADAS; land skin temperature is not analyzed. The vertical distribution of the virtual temperature difference is shown in Figure 17b. During the experiment time period, surface temperature is increased in the AER experiment by up to about $0.5°K$. Note that this warming-up effect is a 6-hourly aggregated result because a 6-hour analysis time-window is applied in the CTL and AER experiments. With regard to the upper air virtual temperature change, we notice that both warming and cooling effects are observed at different atmospheric levels. In the bottom layers over ocean and land, warming is a dominant feature. However, a certain degree of cooling is also seen in upper layers over the ocean. Over land, mostly warming is seen through the whole vertical column. However, the magnitude of the atmospheric virtual temperature difference is about an order of magnitude smaller than the

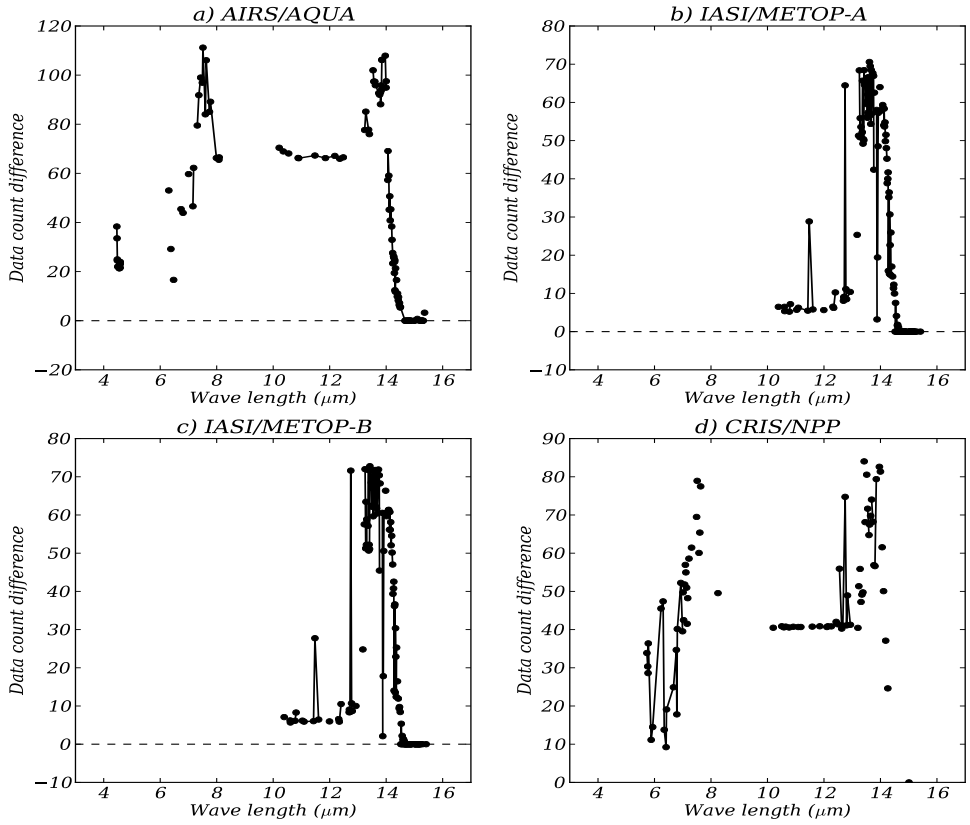

Figure 13: Monthly mean difference of the total number (n) of assimilated observation data in the AER and CTL experiments: $n_{AER} - n_{CTL}$.

surface temperature difference. Thus, most of the BT cooling effect of the AER experiment results in the warming of the surface temperature. In an attempt to validate whether this warmer surface temperature yields a better fit to the observed BT, we compare the OMB and OMA for the CTL and AER experiments with the aid of the skin temperature-sensitive AVHRR channel 4 on METOP-A (see Akella et al. (2016, 2017) for similar validation). Figure 18 compares the OMB and OMA for the CTL experiment. As expected, the OMA is generally smaller than the OMB. Figure 19 shows the same differences for the AER experiment. With the aerosol induced cooling, the OMB is worse off than it was for CTL, though the analysis strives to get closer to the observations. As mentioned above, a future study involving the Jacobians could help explain this increase in surface skin temperature and its connection to the change in BT. Further study with a cycling data assimilation experiment is also required to determine whether these changes are desirable in terms of how they affect the atmospheric model.

4.4 Computational cost

Although the AER experiment shows some improvement in the BT calculation and OMB statistics, the practical application of the CRTM aerosol absorption and scattering option in the quasi-operational run of GEOS-ADAS critically depends on total computational cost. Figure 20 shows

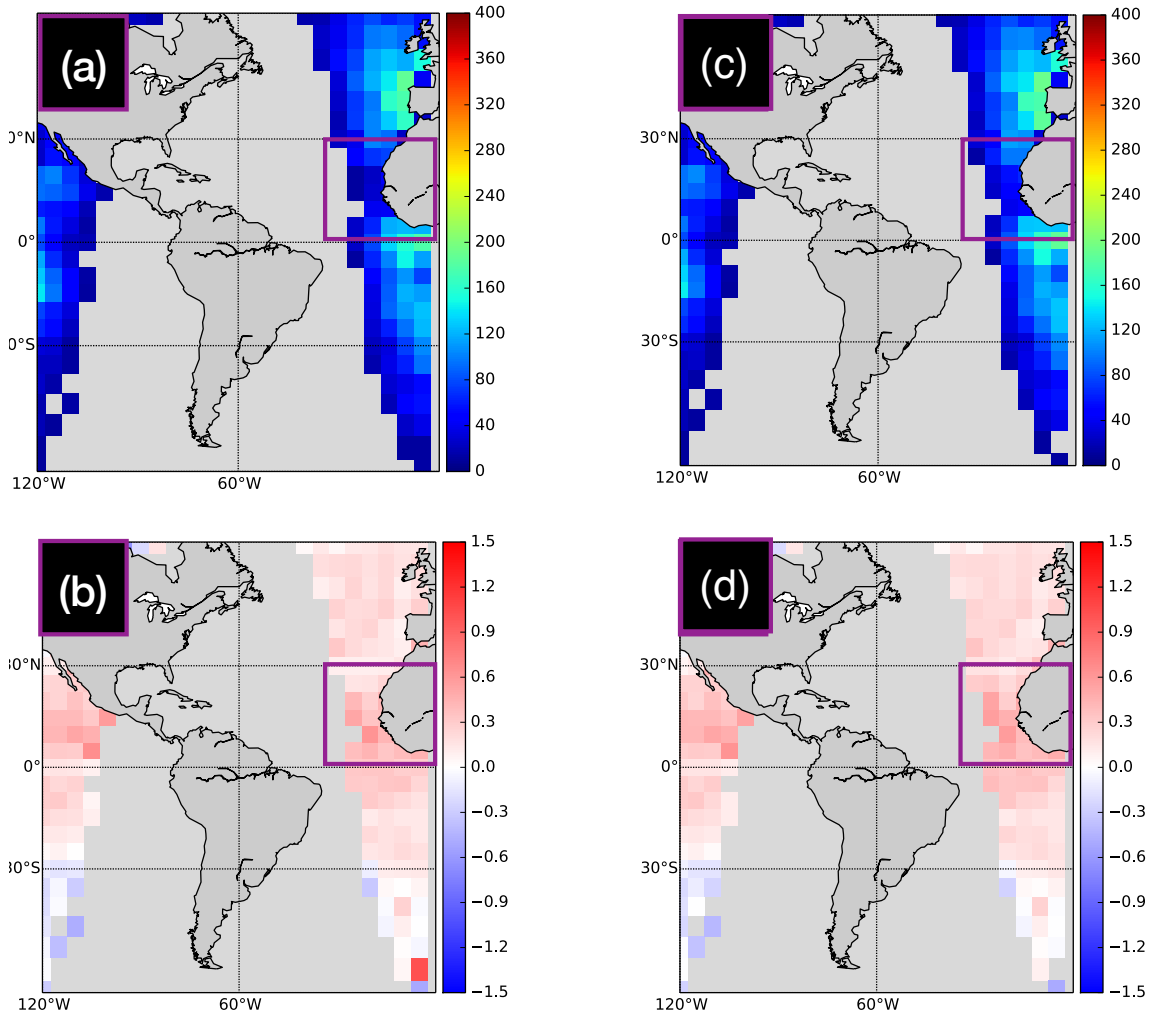

Figure 14: Monthly mean observation counts and OMA after QC and before bias correction for channel number 123 ($11.9\mu m$) of AIRS/AQUA. Top and bottom rows show the number of observations and OMA respectively, binned to a 5^o grid resolution; CTL (a, b) and AER (c, d) experiments are plotted in the left and right columns, respectively. Grid boxes over non-water surfaces and where the observation count was less than 10 have been masked out. The dust maximum in the north Africa region has been highlighted with a purple colored box.

a comparison of the wall-clock time measurements of the CTL and AER experiments for a single analysis run. In the AER experiment, the computational time is more than twice that for CTL for each of the off-line analyses. Most of the computational cost increase is in the so-called observer step (i.e., where the CRTM is called), due to the usage of full three dimensional aerosol concentration fields for fifteen aerosol species in the satellite radiance calculation. Since tens of thousands of data points are used in the assimilation of each satellite instrument, such an increase in computational cost is unacceptable for operational application in the GEOS-ADAS system. Though not examined as part of the present study, the computational cost increase would be even higher in the 4D assimilation setting presently used in the GMAO forward processing systems, in which the background frequency increases to hourly (as opposed to the three-hourly frequency used in

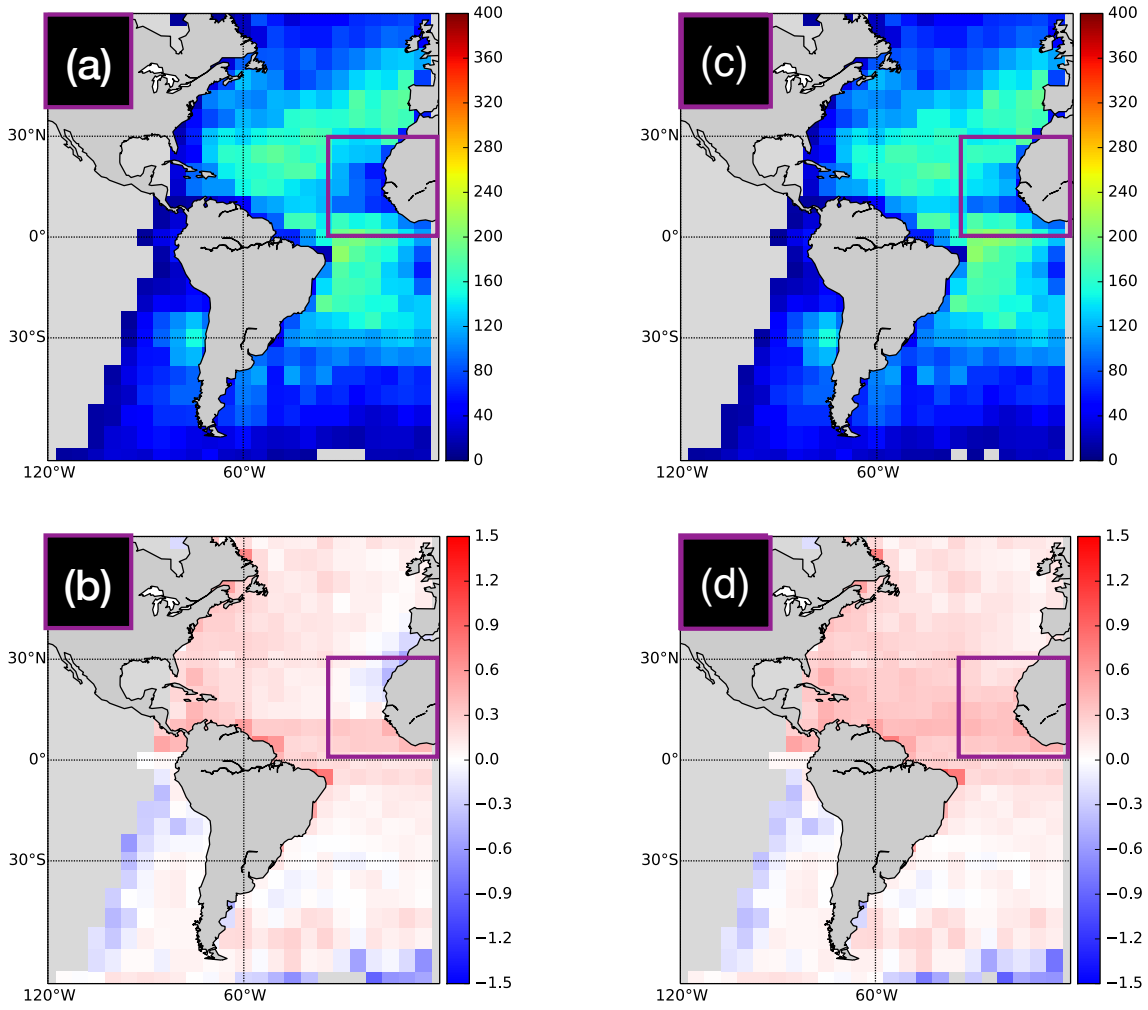

Figure 15: Same as in Figure 14, but for IASI/METOP-A channel number 211 ($10.4\mu m$).

3D settings). Since we observe a strong correlation between the aerosol-affected BT calculation and the two dimensional total AOD field, future work may include the development of a simplified parameterization scheme to facilitate including the aerosol effect in the BT calculation without such high computational cost.

5 Closing Remarks

In this work, we have used version 5.13.2 of GEOS-ADAS, 3DAVR, to investigate the impact of aerosols on the simulation of brightness temperature (BT) for the satellite infrared (IR) instruments currently assimilated into the system. The main experiment performed in this work is an offline, non-cycled experiment designed simply to illustrate how the simulation of BT by the Community Radiative Transfer Model (CRTM) observer calls from the GEOS Gridpoint Statistical Interpolation (GSI) analysis changes when aerosols are allowed to affect the radiative transfer calculations. The aerosol-affected BT so produced were contrasted with the standard, aerosol-blind BT produced in a control experiment. (The control experiment provided the meteorology and aerosol fields for both

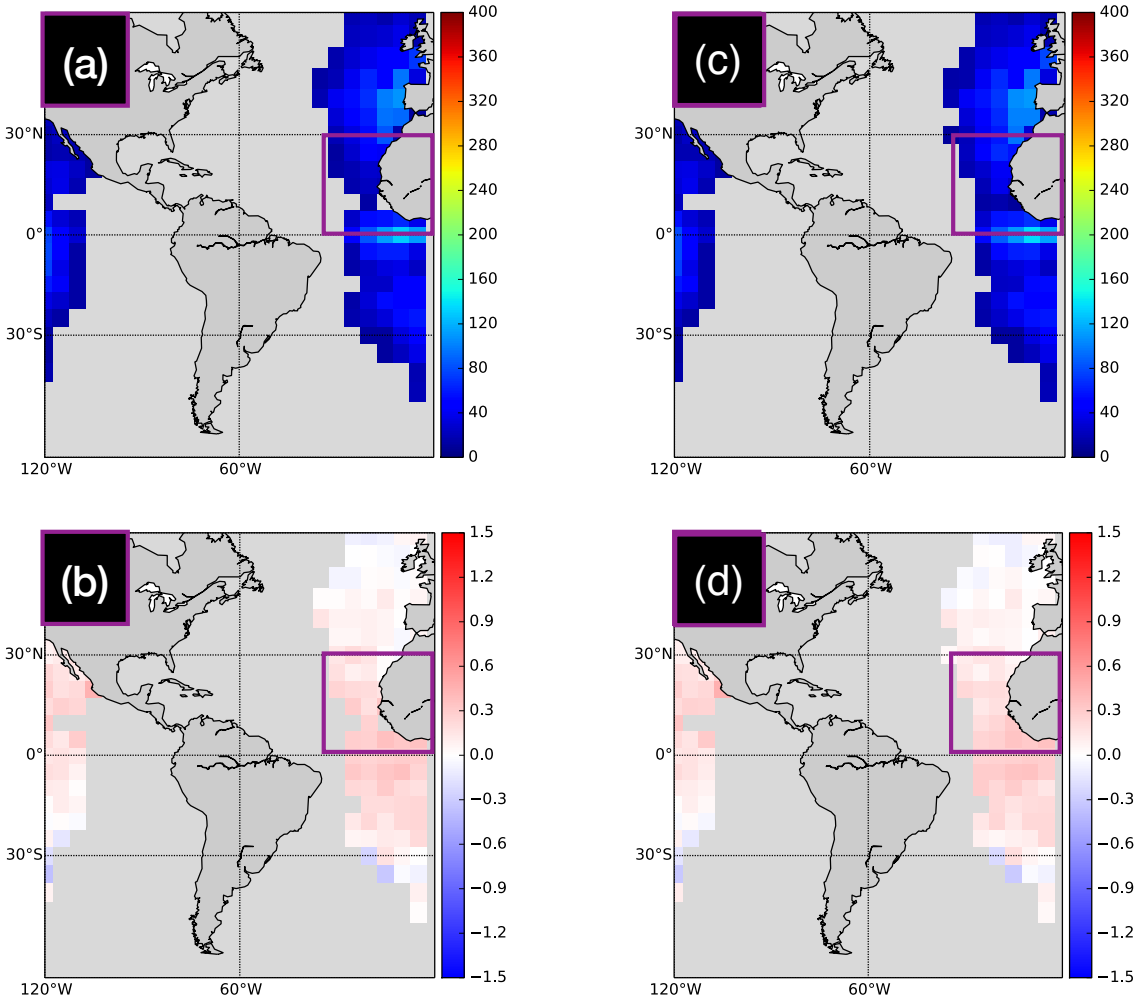

Figure 16: Same as in Figure 14, but for CrIS/NPP channel number 120 ($11.1\mu m$).

the cycled control and the non-cycled experiment.) The aerosols used in this exercise are simulated with the Goddard Chemistry Aerosol Radiation and Transport (GOCART) component of GEOS and are kept realistic by the assimilation of Aerosol Optical Depth (AOD) observations through the Goddard Aerosol Analysis System (GAAS) and Local Displacement Ensemble (LDE) approaches implemented in GEOS-ADAS. The period of August 2016 was chosen for this study because it featured a rather large dust event off the west coast of Africa.

When compared with the aerosol-blind radiative transfer calculations, the aerosol experiment shows a considerable cooling effect on simulated BT. In dust-dominant regions, the cooling effect is about $1.5^{\circ}K$ for the IR atmospheric window channels near the $10\mu m$ wavelength. The magnitudes of this BT cooling effect are comparable to those found in previous related studies (e.g., Weaver et al. (2003), Pierangelo et al. (2004), and Peyridieu et al. (2009)). In carbonaceous and sulfate dominated regions, long-wave channels ($10\sim14\mu m$) are slightly more sensitive to aerosol absorption and scattering, but overall the aerosol impact in these regions is much smaller than it is in dust active regions. In dust active regions, comparison of the horizontal distribution of simulated BT with observations shows that the observed aerosol signal from IR instruments is well captured in the BT calculation. The offline, aerosol-affected experiment highlights a technical issue wherein a

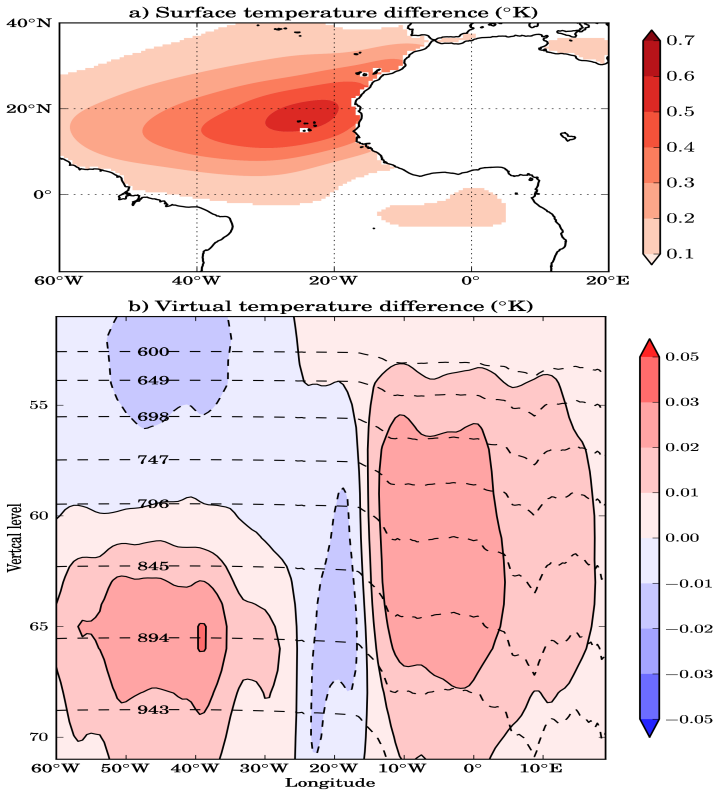

Figure 17: Monthly mean analysis temperature difference of the AER and CTL experiments ($°K$: AER-CTL) in dust active area during August (12:00 UTC) 2016: a) horizontal surface temperature difference b) virtual temperature difference latitudinally averaged between 10°N and 25°N.

non-negligible amount of data is removed from the GSI analysis due to cloud contamination during QC; the version of GSI used in this work handles only clear-sky radiances. Distinguishing aerosol and cloud signals in the QC scheme is a desirable option for GSI but is beyond the scope of the present work.

Stratification of the different aerosol species and their corresponding influences on calculated BTs reveals a strong correlation between the presence of dust and the BT calculations for dust sensitive channels of about $10\mu m$ wavelength. In the shortwave channels, near $4\mu m$ wavelength, the aerosol-cooling effect on BT is not as pronounced. In carbonaceous- and sulfate aerosol regions, a much weaker but similar correlation pattern between simulated BT and AODs is noticed as well. It is evident from this work that dust plays a dominant role in the calculation of aerosol-affected BT, to the point where other species might be acceptably neglected.

Before GSI's QC and bias corrections are applied, the aerosol cooling effect on BT considerably reduces a negative bias in the monthly mean observation-minus-background (OMB) residuals in the dust active region. Over a broad range of channels ($8\sim14\mu m$ wavelength), the positive aerosol impact on the OMB residuals is achieved for most of the high spectral resolution IR instruments. The most beneficial effect is found with CrIS. Although the presence of aerosols somewhat degrades OMB residuals for some of the channels after QC and bias correction, favorable improvements in CrIS are consistently maintained. In addition, the aerosol sensitive channels near $10\mu m$ wavelength continuously show improved OMB residual statistics when using aerosol-affected BTs. The aerosol

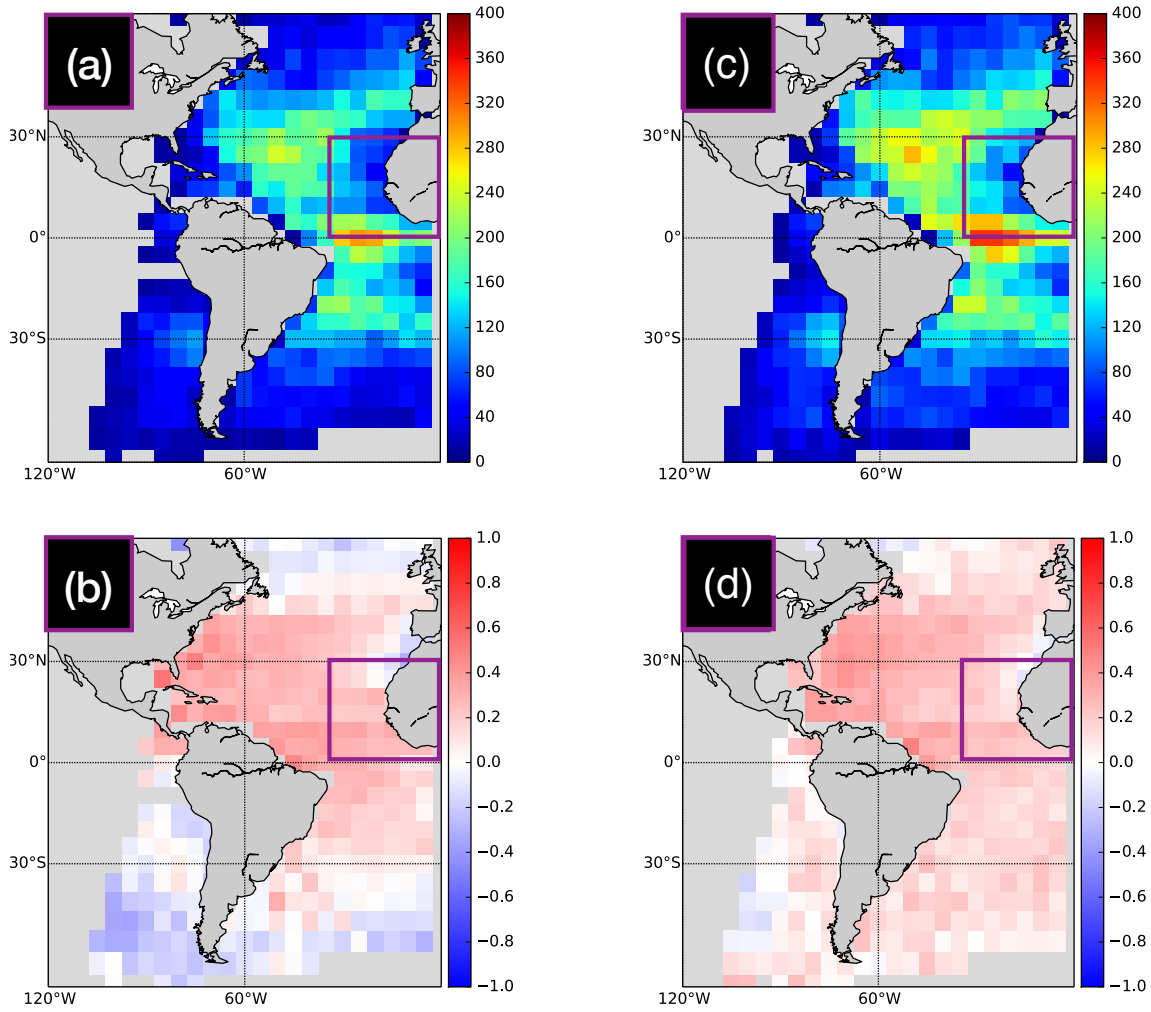

Figure 18: A comparison of the OMB and OMA for skin temperature sensitive channel number 4 of the AVHRR/METOP-A for the CTL experiment, after QC but before applying bias correction, and after binning to a 5^o regular grid. Panels (a) and (b) on left show the number of observations and OMB respectively; corresponding results for OMA are shown in (c) and (d) respectively.

cooling effect on calculated BT leads to a warming of (non-cycled) analyzed surface temperature in the dust transport region over the tropical Atlantic ocean (off north-west Africa). The magnitude of the warming effect is about $0.5°K$ in areas of strong dust activity. Relatively negligible change is observed in the analyzed virtual air temperature; changes in virtual temperature are about an order of magnitude smaller than they are for surface temperature. Future work should investigate the Jacobians of BT sensitivity with respect to temperature fields when aerosols are taken into account. In addition, separately screening the aerosol and cloud mask information in the observation data is expected to contribute further to the accuracy of CRTM's aerosol absorption and scattering scheme when calculating BT.

Computational cost is the most challenging technical issue revealed by this study. The software underlying the current CRTM aerosol absorption and scattering routines does not seem to be computationally efficient enough for practical application. Wall-clock time evaluation shows that the

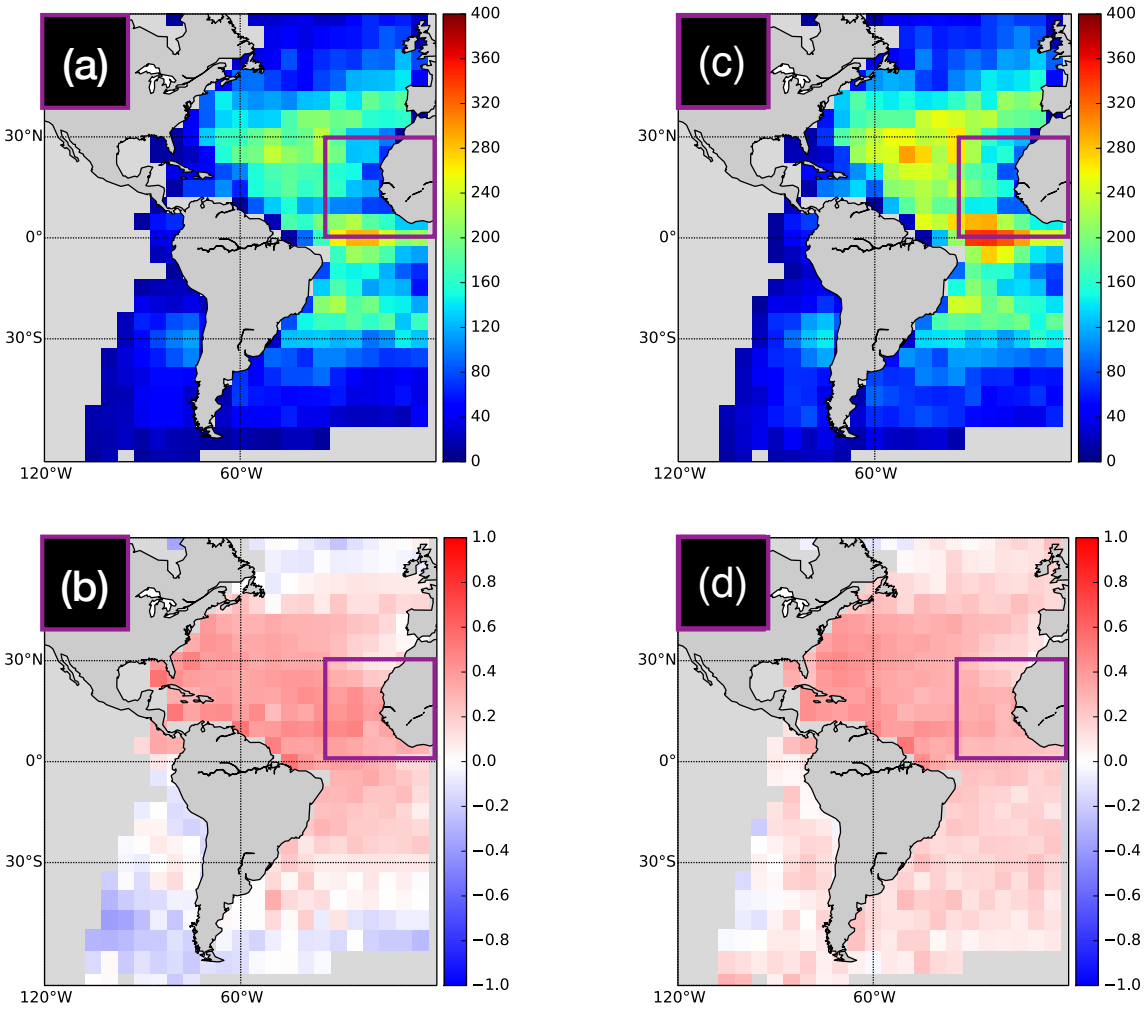

Figure 19: Same as in Figure 18, but for the AER experiment.

application of the CRTM aerosol absorption and scattering option more than doubles the computational time of the analysis. The large increase in computational cost appears to be unjustifiable in a practical setting given the modest impacts shown here. A possible approach to reducing the computational cost might involve an optimally controlled temporal interpolation of aerosol background information and limiting the application of the CRTM aerosol absorption and scattering option to only the most influential aerosol species.

We hope this work provides useful information on the problems that still need to be addressed before aerosol-affected BT calculations can be reliably and efficiently used in a GSI-based analysis system.

6 Acknowledgments

We thank Gary Partyka for helping us in identifying the dates and regions of intense aerosol/dust activity. Computations were performed on the Discover cluster of the NASA Center for Computational Sciences (NCCS) at the Goddard Space Flight Center.

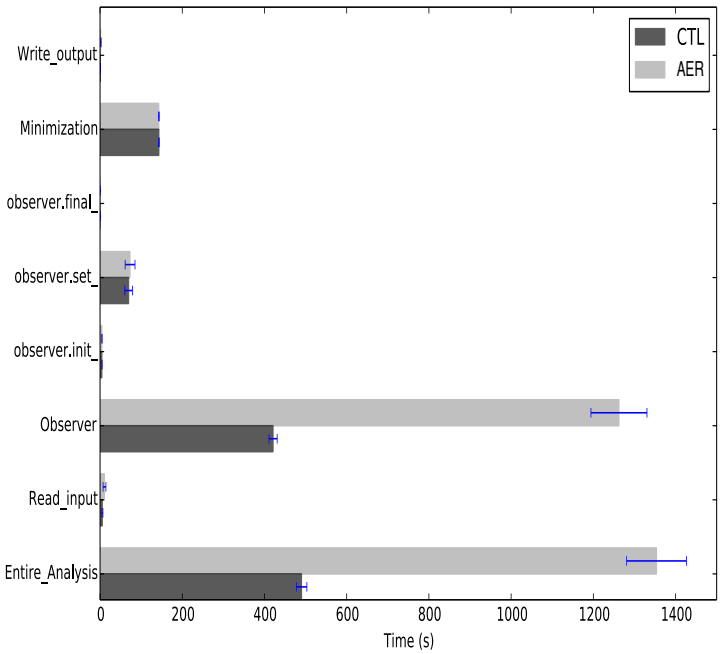

Figure 20: Wall-clock time measurements of the CTL and AER experiments for single analysis run.

References

Akella, S., Todling, R., and Suarez, M. (2016). Estimation of the ocean skin temperature using the NASA GEOS Atmospheric Data Assimilation System. Technical Report Series on Global Modeling and Data Assimilation NASA/TM-2016-104606/Vol 44, NASA Goddard Space Flight Center.

Akella, S., Todling, R., and Suarez, M. (2017). Assimilation for skin SST in the NASA GEOS atmospheric data assimilation system. *Quarterly Journal of the Royal Meteorological Society*, 143(703):1032–1046.

Bloom, S. C., Takacs, L. L., da Silva, A. M., and Ledvina, D. (1996). Data assimilation using incremental analysis updates. *Mon Weather Rev*, 124:1256–1271.

Boucher, O., Randall, D., Artaxo, P., Bretherton, C., Feingold, G., Forster, P., Kerminen, V. M., Kondo, Y., Liao, H., Lohmann, U., Rasch, P., Satheesh, S. K., Sherwood, S., Stevens, B., and Zhang, X. Y. (2013). *Clouds and Aerosols*, book section 7, page 571658. Cambridge University Press, Cambridge, United Kingdom and New York, NY, USA.

Buchard, V., da Silva, A. M., Colarco, P. R., Darmenov, A., Randles, C. A., Govindaraju, R., Torres, O., Campbell, J., and Spurr, R. (2015). Using the omi aerosol index and absorption aerosol optical depth to evaluate the NASA MERRA Aerosol Reanalysis. *Atmospheric Chemistry and Physics*, 15(10):57435760.

Buchard, V., da Silva, A. M., Randles, C. A., Colarco, P. R., Ferrare, R., Hair, J., Hostetler, C., Tackett, J., and Winker, D. (2016). Evaluation of the surface pm2.5 in version 1 of the NASA MERRA Aerosol Reanalysis over the united states. *Atmospheric Environment*, 125:100111.

Colarco, P. R., da Silva, A. M., Chin, M., and Diehl, T. (2010). Online simulations of global aerosol distributions in the NASA GEOS-4 model and comparisons to satellite and ground-based aerosol optical depth. *Journal of Geophysical Research*, 115(D14).

Gelaro, R. and coauthors (2017). The modern-era retrospective analysis for research and applications, version 2 (MERRA-2). *J. Climate*, 30:1–1.

Kleist, D. T., Parrish, D. F., Derber, J. C., Treadon, R., Wu, W. S., and Lord, S. (2009). Introduction of the GSI into the NCEP Global Data Assimilation System. *Weather and Forecasting*, 24(6):16911705.

Liu, Q., Han, Y., van Delst, P., and Weng, F. (2007). Modeling aerosol radiance for NCEP Data Assimilation. In *Fourier Transform Spectroscopy/ Hyperspectral Imaging and Sounding of the Environment*, page HThA5. Optical Society of America.

Lynch, P., Reid, J. S., Westphal, D. L., Zhang, J., Hogan, T. F., Hyer, E. J., Curtis, C. A., Hegg, D. A., Shi, Y., Campbell, J. R., and et al. (2016). An 11-year global gridded aerosol optical thickness reanalysis (v1.0) for atmospheric and climate sciences. *Geoscientific Model Development*, 9(4):14891522.

Massart, S. M., Pajot, B., Piacentini, A., and Pannekoucke, O. (2010). On the merits of using a 3d-fgat assimilation scheme with an outer loop for atmospheric situations governed by transport. *Mon. Wea. Rev.*, 138:4509–4522.

Merchant, C. J., Embury, O., Borgne, P. L., and Bellec, B. (2006). Saharan dust in nighttime thermal imagery: Detection and reduction of related biases in retrieved sea surface temperature. *Remote Sensing of Environment*, 104(1):15 – 30.

Morcrette, J.-J., Boucher, O., Jones, L., Salmond, D., Bechtold, P., Beljaars, A., Benedetti, A., Bonet, A., Kaiser, J. W., Razinger, M., and et al. (2009). Aerosol analysis and forecast in the European Centre for Medium-Range Weather Forecasts Integrated Forecast System: Forward modeling. *Journal of Geophysical Research*, 114(D6).

Peyridieu, S., Chdin, A., Tanr, D., Capelle, V., Pierangelo, C., Lamquin, N., and Armante, R. (2009). Saharan dust infrared optical depth and altitude retrieved from AIRS: a focus over North Atlantic comparison to MODIS and CALIPSO. *Atmospheric Chemistry and Physics Discussions*, 9(5):2119921235.

Pierangelo, C., Chdin, A., Heilliette, S., Jacquinet-Husson, N., and Armante, R. (2004). Dust altitude and infrared optical depth from AIRS. *Atmospheric Chemistry and Physics*, 4(7):18131822.

Putman, W. M. and Lin, S.-J. (2007). Finite-volume transport on various cubed-sphere grids. *Journal of Computational Physics*, 227(1):5578.

Randles, C. A., da Silva, A. M., Buchard, V., Darmenov, A., P. R. Colarco, V. A., Bian, H., Nowottnick, E. P., Pan, X., Smirnov, A., Yu, H., and Govindaraju, R. (2016). MERRA-2 aerosol assimilation. Technical Report Series on Global Modeling and Data Assimilation NASA/TM2016-104606/Vol 45, NASA Goddard Space Flight Center.

Weaver, C. J., Joiner, J., and Ginou, P. (2003). Mineral aerosol contamination of TIROS Operational Vertical Sounder (TOVS) temperature and moisture retrievals. *Journal of Geophysical Research*, 108(D8).

Appendix A. Acronyms

ADAS atmospheric data assimilation system

AERONET Aerosol Robotic Network

AGCM atmospheric general circulation model

AIRS Advanced Infrared Sounder

AOD Aerosol Optical Depth

AVHRR Advanced Very High Resolution Radiometer

BC black carbon

BT brightness temperature

CALIOP Cloud Aerosol Lidar with Orthogonal Polarization

cMass column mass

CrIS Cross-track Infrared Sounder

CRTM Community Radiative Transfer Model

ECMWF European Center for Medium-Range Weather Forecasts

FP Forward Processing

FGAT First-Guess at the Appropriate Time

GAAS Goddard Aerosol Analysis System

GEOS Goddard Earth Observing System

GOCART Goddard Chemistry, Aerosol, Radiation, and Transport

GMAO Global Modeling and Assimilation Office

GOCART Goddard Chemistry Aerosol Radiation and Transport

GSI Gridpoint Statistical Interpolation

HIRS High resolution Infrared Radiation Sounder

IASI Infrared Atmospheric Sounding Interferometer

IR infrared

LDE Local Displacement Ensemble

MISR Multi-angle Imaging SpectroRadiometer

MODIS MODerate Resolution Imaging Spectroradiometer

MW	microwave
NRL	Naval Research Laboratory
OC	organic carbon
OMA	observation-minus-analysis
OMB	observation-minus-background
PSAS	Physical-space Statistical Analysis System
QC	quality control
SEVIRI	Spinning Enhanced Visible and Infrared Imager
SST	sea surface temperature
TOVS	TIROS Operational Vertical Sounder

Previous Volumes in This Series

Volume 1 *September 1994*
Documentation of the Goddard Earth Observing System (GEOS) general circulation model - Version 1
L. L. Takacs, A. Molod, and T. Wang

Volume 2 *October 1994*
Direct solution of the implicit formulation of fourth order horizontal diffusion for gridpoint models on the sphere
Y. Li, S. Moorthi, and J. R. Bates

Volume 3 *December 1994*
An efficient thermal infrared radiation parameterization for use in general circulation models
M.-D. Chou and M. J. Suarez

Volume 4 *January 1995*
Documentation of the Goddard Earth Observing System (GEOS) Data Assimilation System - Version 1
James Pfaendtner, Stephen Bloom, David Lamich, Michael Seablom, Meta Sienkiewicz, James Stobie, and Arlindo da Silva

Volume 5 *April 1995*
Documentation of the Aries-GEOS dynamical core: Version 2
Max J. Suarez and Lawrence L. Takacs

Volume 6 *April 1995*
A Multiyear Assimilation with the GEOS-1 System: Overview and Results
Siegfried Schubert, Chung-Kyu Park, Chung-Yu Wu, Wayne Higgins, Yelena Kondratyeva, Andrea Molod, Lawrence Takacs, Michael Seablom, and Richard Rood

Volume 7 *September 1995*
Proceedings of the Workshop on the GEOS-1 Five-Year Assimilation
Siegfried D. Schubert and Richard B. Rood

Volume 8 *March 1996*
Documentation of the Tangent Linear Model and Its Adjoint of the Adiabatic Version of the NASA GEOS-1 C-Grid GCM: Version 5.2
Weiyu Yang and I. Michael Navon

Volume 9 *March 1996*
Energy and Water Balance Calculations in the Mosaic LSM
Randal D. Koster and Max J. Suarez

Volume 10 *April 1996*
Dynamical Aspects of Climate Simulations Using the GEOS General Circulation Model
Lawrence L. Takacs and Max J. Suarez

Volume 11 *May 1997*
Documentation of the Tangent Linear and its Adjoint Models of the Relaxed Arakawa-Schubert Moisture Parameterization Package of the NASA GEOS-1 GCM (Version 5.2)
Weiyu Yang, I. Michael Navon, and Ricardo Todling

Volume 12 *August 1997*
Comparison of Satellite Global Rainfall Algorithms
Alfred T. C. Chang and Long S. Chiu

Volume 13 Interannual Variability and Potential Predictability in Reanalysis Products
December 1997 **Wie Ming and Siegfried D. Schubert**

Volume 14 A Comparison of GEOS Assimilated Data with FIFE Observations
August 1998 **Michael G. Bosilovich and Siegfried D. Schubert**

Volume 15 A Solar Radiation Parameterization for Atmospheric Studies
June 1999 **Ming-Dah Chou and Max J. Suarez**

Volume 16 Filtering Techniques on a Stretched Grid General Circulation Model
November 1999 **Lawrence Takacs, William Sawyer, Max J. Suarez, and Michael S. Fox-Rabinowitz**

Volume 17 Atlas of Seasonal Means Simulated by the NSIPP-1 Atmospheric GCM
July 2000 **Julio T. Bacmeister, Philip J. Pegion, Siegfried D. Schubert, and Max J. Suarez**

Volume 18 An Assessment of the Predictability of Northern Winter Seasonal Means with the NSIPP1 AGCM
December 2000 **Philip J. Pegion, Siegfried D. Schubert, and Max J. Suarez**

Volume 19 A Thermal Infrared Radiation Parameterization for Atmospheric Studies
July 2001 **Ming-Dah Chou, Max J. Suarez, Xin-Zhong, and Michael M.-H. Yan**

Volume 20 The Climate of the FVCCM-3 Model
August 2001 **Yehui Chang, Siegfried D. Schubert, Shian-Jiann Lin, Sharon Nebuda, and Bo-Wen Shen**

Volume 21 Design and Implementation of a Parallel Multivariate Ensemble Kalman Filter for the Poseidon Ocean General Circulation Model
September 2001 **Christian L. Keppenne and Michele M. Rienecker**

Volume 22 Coupled Ocean-Atmosphere Radiative Model for Global Ocean Biogeochemical Models
August 2002 **Watson W. Gregg**

Volume 23 Prospects for Improved Forecasts of Weather and Short-term Climate Variability on Subseasonal (2-Week to 2-Month) Time Scales
November 2002 **Siegfried D. Schubert, Randall Dole, Huang van den Dool, Max J. Suarez, and Duane Waliser**

Volume 24 Temperature Data Assimilation with Salinity Corrections: Validation for the NSIPP Ocean Data Assimilation System in the Tropical Pacific Ocean, 1993–1998
July 2003 **Alberto Troccoli, Michele M. Rienecker, Christian L. Keppenne, and Gregory C. Johnson**

Volume 25 Modeling, Simulation, and Forecasting of Subseasonal Variability
December 2003 **Duane Waliser, Siegfried D. Schubert, Arun Kumar, Klaus Weickmann, and Randall Dole**

Volume 26 *April 2005*
Documentation and Validation of the Goddard Earth Observing System (GEOS) Data Assimilation System - Version 4
Senior Authors: S. Bloom, A. da Silva and D. Dee
Contributing Authors: M. Bosilovich, J-D. Chern, S. Pawson, S. Schubert, M. Sienkiewicz, I. Stajner, W-W. Tan, and M-L. Wu

Volume 27 *December 2008*
The GEOS-5 Data Assimilation System - Documentation of Versions 5.0.1, 5.1.0, and 5.2.0
M. M. Rienecker, M. J. Suarez, R. Todling, J. Bacmeister, L. Takacs, H.-C. Liu, W. Gu, M. Sienkiewicz, R. D. Koster, R. Gelaro, I. Stajner, and J. E. Nielsen

Volume 28 *April 2012*
The GEOS-5 Atmospheric General Circulation Model: Mean Climate and Development from MERRA to Fortuna
Andrea Molod, Lawrence Takacs, Max Suarez, Julio Bacmeister, In-Sun Song, and Andrew Eichmann

Volume 29 *May 2012*
Atmospheric Reanalyses Recent Progress and Prospects for the Future. A Report from a Technical Workshop, April 2010
Michele M. Rienecker, Dick Dee, Jack Woollen, Gilbert P. Compo, Kazutoshi Onogi, Ron Gelaro, Michael G. Bosilovich, Arlindo da Silva, Steven Pawson, Siegfried Schubert, Max Suarez, Dale Barker, Hirotaka Kamahori, Robert Kistler, and Suranjana Saha

Volume 30 *September 2012*
The GEOS-ODAS, Description and Evaluation
Guillaume Vernieres, Michele M. Rienecker, Robin Kovach and Christian L. Keppenne

Volume 31 *March 2013*
Global Surface Ocean Carbon Estimates in a Model Forced by MERRA
Watson W. Gregg, Nancy W. Casey, and Cécile S. Rousseaux

Volume 32 *March 2014*
Estimates of AOD Trends (2002–2012) over the World's Major Cities based on the MERRA Aerosol Reanalysis
Simon Provençal, Pavel Kishcha, Emily Elhacham, Arlindo M. da Silva and Pinhas Alpert

Volume 33 *August 2014*
The Effects of Chlorophyll Assimilation on Carbon Fluxes in a Global Biogeochemical Model
Cécile S. Rousseaux and Watson W. Gregg

Volume 34 *September 2014*
Background Error Covariance Estimation using Information from a Single Model Trajectory with Application to Ocean Data Assimilation into the GEOS-5 Coupled Model
Christian L. Keppenne, Michele M. Rienecker, Robin M. Kovach, and Guillaume Vernieres

Volume 35 *December 2014*
Observation-Corrected Precipitation Estimates in GEOS-5
Rolf H. Reichle and Qing Liu

Volume 36 Evaluation of the 7-km GEOS-5 Nature Run
March 2015 **Ronald Gelaro, William M. Putman, Steven Pawson, Clara Draper, Andrea Molod, Peter M. Norris, Lesley Ott, Nikki Privé, Oreste Reale, Deepthi Achuthavarier, Michael Bosilovich, Virginie Buchard, Winston Chao, Lawrence Coy, Richard Cullather, Arlindo da Silva, Anton Darmenov, Ronald M. Errico, Marangelly Fuentes, Min-Jeong Kim, Randal Koster, Will McCarty, Jyothi Nattala, Gary Partyka, Siegfried Schubert, Guillaume Vernieres, Yuri Vikhliaev, and Krzysztof Wargan**

Volume 37 Maintaining Atmospheric Mass and Water Balance Within Reanalysis
March 2015 **Lawrence L. Takacs, Max Suarez, and Ricardo Todling**

Volume 38 The Quick Fire Emissions Dataset (QFED): Documentation of versions 2.1, 2.2 and 2.4
September 2015 **Anton Darmenov and Arlindo da Silva**

Volume 39 Land Boundary Conditions for the Goddard Earth Observing System Model Version 5 (GEOS-5) Climate Modeling System - Recent Updates and Data File Descriptions
September 2015 **Sarith Mahanama, Randal Koster, Gregory Walker, Lawrence Takacs, Rolf Reichle, Gabrielle De Lannoy, Qing Liu, Bin Zhao, and Max Suarez**

Volume 40 Soil Moisture Active Passive (SMAP) Project Assessment Report for the Beta-Release L4_SM Data Product
October 2015 **Rolf H. Reichle, Gabrielle J. M. De Lannoy, Qing Liu, Andreas Colliander, Austin Conaty, Thomas Jackson, John Kimball, and Randal D. Koster**

Volume 41 GDIS Workshop Report
October 2015 **Schubert, Siegfried, Will Pozzi, Kingtse Mo, Eric Wood, Kerstin Stahl, Mike Hayes, Juergen Vogt, Sonia Seneviratne, Ron Stewart, Roger Pulwarty, and Robert Stefanski**

Volume 42 Soil Moisture Active Passive (SMAP) Project Calibration and Validation for the L4_C Beta-Release Data Product
November 2015 **John Kimball, Lucas Jones, Joseph Glassy, E. Natasha Stavros, Nima Madani, Rolf Reichle, Thomas Jackson, and Andreas Colliander**

Volume 43 MERRA-2: Initial Evaluation of the Climate
September 2015 **Michael G. Bosilovich, Santha Akella, Lawrence Coy, Richard Cullather, Clara Draper, Ronald Gelaro, Robin Kovach, Qing Liu, Andrea Molod, Peter Norris, Krzysztof Wargan, Winston Chao, Rolf Reichle, Lawrence Takacs, Yury Vikhliaev, Steve Bloom, Allison Collow, Stacey Firth, Gordon Labow, Gary Partyka, Steven Pawson, Oreste Reale, Siegfried D. Schubert, and Max Suarez**

Volume 44 Estimation of the Ocean Skin Temperature using the NASA GEOS Atmospheric Data Assimilation System
February 2016 **Santha Akella, Ricardo Todling and Max Suarez**

Volume 45
December 2016

The MERRA-2 Aerosol Assimilation. NASA Technical Report Series on Global Modeling and Data Assimilation

C. A. Randles, A. M. da Silva, V. Buchard, A. Darmenov, P. R. Colarco, V. Aquila, H. Bian, E. P. Nowottnick, X. Pan, A. Smirnov, H. Yu, and R. Govindaraju

Volume 46
October 2016

MERRA-2 Input Observations: Summary and Assessment

Will McCarty, Lawrence Coy, Ronald Gelaro, Albert Huang, Dagmar Merkova, Edmond B. Smith, Meta Seinkiewicz, and Krzysztof Wargan

Volume 47
May 2017

An Evaluation of Teleconnections Over the United States in an Ensemble of AMIP Simulations with the MERRA-2 Configuration of the GEOS Atmospheric Model

Allison B. Marquardt Collow, Sarith P. Mahanama, Michael G. Bosilovich, Randal D. Koster, and Siegfried D. Schubert

Volume 48
July 2017

Description of the GMAO OSSE for Weather Analysis Software Package: Version 3

Ronald M Errico, Nikki C. Privé, David Carvalho, Meta Sienkiewicz, Amal El Akkraoui, Jing Guo, Ricardo Todling, Will McCarty, William M. Putman, Arlindo da Silva, Ronald Gelaro, Isaac Moradi